OPTIMAL CONTROL OF DISTRIBUTION NETWORKS

FAYAS AHAMED MOHAMED HASAN

A THESIS SUBMITTED TO THE FACULTY OF GRADUATE STUDIES
IN PARTIAL FULFILMENT OF THE REQUIREMENTS FOR THE
DEGREE OF

MASTER OF APPLIED SCIENCE

DEPARTMENT OF ELECTRICAL AND COMPUTER ENGINEERING
YORK UNIVERSITY
TORONTO, ONTARIO
AUGUST 2021

Abstract

The recent proliferation of distributed energy resources at the distribution level of the electricity grid has altered the landscape of power sector. The power output of these generation units depends on the geographic and atmospheric condition, thus highly variable. Moreover these sources are integrated to distribution feeder via power electronic based converters which lacks mechanical inertia to instantaneously counter voltage fluctuations occurring in the grid. While the source side is populated by these stochastic based generations, demand side is now dictated by sophisticated power electronic based devices which requires a higher voltage quality for reliable operation. The existing state-of-the-art techniques are proven to be ineffective in tacking this voltage control issue in the modern distribution grid. This thesis presents a network reduction based controller design approach to overcome these challenges. The effectiveness of this algorithm is validated by theoretical justifications and practical simulations on 136-Brazilian test system.

Acknowledgements

I feel a deep sense of humbleness and gratitude towards my thesis advisor Prof. Pirathayini Srikantha for her motivation, encouragement and support during my graduate studies. Her guidance has helped me in many ways to enhance my research and professional skills and it's always a pleasure to work with her.

Many thanks to my thesis examination committee members, Prof. Afshin Rezaei Zare and Prof. Marina Freire-Gormaly for generously offering their time and valuable suggestions to improve my thesis.

Financial support from York University, Faculty of Graduate Studies and Natural Sciences and Engineering Research Council of Canada (NSERC) are greatly appreciated.

Last but not least, I would like to thank to my family and friends. My heartfelt thanks to my parents and siblings for their love and support while I was pursuing my studies in Canada. Many thanks to my friends in London and Toronto, who have been extremely supportive and being there for me at times of hardship.

Table of Contents

List of Tables

List of Figures

Abbreviations

RES	renewable energy sources
DER	distributed energy resources
MV	medium voltage
LV	low voltage
DN	distribution network
EV	electric vehicle
VVC	volt-var controllers
LQR	linear quadratic regulator
ARE	algebraic Riccati equations
P&Q	active and reactive power
V&f	voltage and frequency
SD	semi-definite
PV	photovoltaic
OCP	optimal control problem
DP	dynamic programming
GPS	global positioning system
VSC	voltage source converters
PMU	phasor measurement units
PWM	pulse width modulation
OPF	optimal power flow
ADMM	alternating direction method of multipliers
SDP	semi-definite programming

List of Symbols

- $(.)^T$, $(.)^*$, $(.)^{-1}$ and $\| \, . \, \|_2$: Transpose, conjugate, inverse and L^2-norm operators.
- $\mathcal{N} = \{1, ..., n\}, \mathcal{E} \subseteq \mathcal{N} \times \mathcal{N}$ and $\mathcal{A} = (a_{ij}) \in \mathbb{R}^{n \times n}$: The node set, edge set and adjacency matrix of a graph.
- $\mathcal{G} = \{\mathcal{N}, \mathcal{E}, \mathcal{A}\}$: An undirected graph.
- λ_{max}^M, $M_{nm} \in \mathbb{C}^{n \times m}$, $\mathbf{sum}(M)$ and $\overline{M}$: The greatest eigenvalue, a block matrix , element-wise algebraic summation, element-by-element conjugation of complex valued matrix M.
- $\text{diag}(x_i) \in \mathbb{R}^{n \times n}$: The proper diagonal matrix with corresponding entries x_is

Chapter 1

Introduction

Rising concerns on climate change and energy independence have drawn much attention towards RES during the last two decades. Except for the emissions during its manufacturing process (emissions/energy produced is negligible) and the metallic residuals after the decommissioning of the plants, RES do not contribute to global warming/environmental pollution during its operation. Multiple countries have ramped up addition of RES to the electricity generation mix and there were instances reported form countries like Netherlands where electricity produced by RES surpassed the national power demand. Popular examples for RES include solar photovoltaic power plants, wind turbines, geothermal power plants, wave energy generators etc.

DER include RES, EV, Energy storages (e.g. batteries, fly wheels), controllable loads (i.e. the load of particular consumers which under contract must be reduced, for a limited period of time, at the request of the utility) etc. These DERs are connected to the electricity grid at the MV and LV distribution levels via power electronic convertors such as inverters. Thus, the increased integration of DER results in stochastic bi-directional power flow throughout the feeder, while the DN is originally designed for uni-directional power flow. Moreover a DN with few MWs of capacity can consist of hundreds of nodes with fast varying loads connected to it.

These will results in V and f fluctuations in the DN. For example, if the DER is based on solar PV, system loading can change in time scales of seconds resulting in voltage rise and increased penetration EV loading can results in voltage plunge. Unfortunately the DER converters do not offer 'inertial' response (which is an inherent feature of large scale synchronous generators) to counter these sudden changes in voltage and frequency. Moreover voltage and frequency control in DN is a

coupled problem due to the higher resistive to reactance ratio (R/X) of the distribution lines.

The existing state-of-the-art technology which is the VVC is proven to be ineffective in providing voltage regulation for the modern grid and it is shown to degrade the power quality. Moreover, the structure of the DN is not expected to change at a pace to accommodate the impending changes in the sources and loads. Past experiences and simulations of future scenarios [4] show this will result in serious consequences such as significant DER curtailment and blackouts. Thus, the existing power DN requires efficient, robust, scalable and reliable control techniques to tackle those issues. This aim of this thesis is to explore few such techniques and to propose a novel addition to the existing state-of-the art.

1.1 Literature Review

The V and f control in the transmission network is performed by large scale centralised generation units such as coal power plants, hydro power plants etc. The generator governor in these power plants is essentially responsible for frequency control while maintaining the proportional power sharing amongst the power plants and automatic voltage regulators (such as shunt capacitors, shunt reactors and static var compensators) and transformer automatic tap changers are primarily maintain the voltage with the prescribed bandwidth [5]. In the modern grid, as the generating units are becoming decentralised and concentrated towards the DN, these conventional approaches were proven to be ineffective in V and f control. Although in the high voltage transmission network the V and f are controlled independently by various methods mentioned above, V and f control is a coupled problem for the MV and LV DN due to the higher R/X ratio of the distribution feeders.

The existing control literature consists of wide range of control techniques to address this issue. Inspired by synchronous generators, droop control and its derivates [6, 7, 8, 9, 10] are the most popular communication-free control technique that is proven to be effective for power electronics based decentralised generations. Droop control linearly trades off active and reactive power with voltage and frequency for parallel operation of generators [11]. That is the controller adjust active and reactive power output respectively, based on a linear relation when a change in voltage and frequency is observed. The conventional droop laws assume V and f control problems to be independent to each other while for the LV and MV network it's a coupled problem. Moreover

this control technique focuses only on local control objectives which can result in inefficiencies (for example, global optimal conditions such as reducing the cost of power, lines losses etc).

In the recent works [7, 2, 10], researchers address this issue by incorporating optimality conditions with the droop laws. In all these works, no emphasis was given to voltage regulation. Moreover, in [2] the tight coupling among P and Q which is induced by non-zero line resistance is not accounted for in the droop expressions. Authors of [7], utilise the infinite horizon LQR along with droop laws which results in solving continuous-time ARE. Authors in [7] propose expensive iterative techniques such as in [12] to solve the ARE, which can result in intractability of the problem. A similar challenge is observed with the decentralized control technique presented in [13], as authors do not provide a tractable method to solve the Lyapunov matrix equation resulting from the optimality condition.

Communication based control techniques can be loosely classified as *centralized* and *decentralized* strategies. *Centralized* control relies on a single central entity which is responsible of monitoring and computing actuation signals. Although this control is proven to achieve global objectives (ie, minimize cost of power supplied etc), single point of failure can cause total system collapse. Moreover these centralised control techniques are subjected to computational and communication overheads. Thus this is proven to be slow and occurring over larger time horizons in performing actuating command to the dispatching entitles [14]. *Decentralized* control overcomes this issue by enriching individual subsystems to monitor and perform measurements and localised control actions. Seminal work has been carried out in the recent past on communication based decentralised control and coordination of LV/MV networks [15, 16, 14]. Reference [15] proposes a SD relaxation solution to tackle the optimal non-convex distributed voltage regulation problem in the DN. Although the resulting SD problem is convex, the rank-1 constraint on voltage outer product matrix is omitted in the problem formation, which can result in infeasible solutions. A similar relaxation technique has been used in [16] to solve the distributed power flow problem in the DN. Although authors in [14] overcome this issue by proposing exact convex relaxations using S-procedure, system dynamics are not taken into account when formulating the optimal decentralized coordination problem.

1.2 Problem statement and thesis objectives

The modern DN is facing changes in both source and demand side. On the source end there is an increasing integration of power electronic based sustainable energy sources like Solar PV, wind turbines etc. Due to the clean energy incentive programs by various governments [14], consumers can now actively participate in energy trade (by net metering option on rooftop Solar PV and EV battery discharging to the grid during the peak hours known as V2G) forming a prosumer based DN. This results in bi-directional power flow at various nodes throughout the distribution feeder which is originally designed for unidirectional power flow. Moreover the system loading at those nodes could be highly variable due to the interminable nature of DERs (can change in seconds time scale if the DER is Solar PV based). This can result in voltage fluctuations and degrade the quality of system voltage violating operational limits outlined the IEEE 1547 standard. Whereas the voltage could potentiality degrade due to the increasing DERs, the voltage quality required to reliably operate the loads is increasing, as a result of increased penetration of power electronics on the demand side [14]. The existing state-of-the-art which is VVC are not effective in tackling this issue as voltage control is performed by static devices such as capacitor banks, transformer tap changers etc. Although communication based techniques are proven to counter this issue, computation and communication overheads, scalability, tackling the non-convexities resulting from the power flow and constraints on the voltage and achieving economically optimal operating points are challenges to be addressed. In light of these issues, the objectives of thesis are listed below:

- Formulating the control problem for an active DN as an optimisation problem for a finite time horizon.
- Applying appropriate network reduction techniques to eliminate passive elements in the DN to enhance scalability of the algorithm.
- Decomposing the OCP into sub problems in spatial and temporal domains so that exact convex relaxations can be applied to overcome the non-convexities.
- Demonstrating the feasibility, convergence and scalability of the proposed algorithm via theoretical studies and practical simulations.

1.3 Thesis outline

The rest of the thesis chapters discuss the methodologies used to achieve the objectives outlined above. Brief descriptions of imminent chapters are listed below:

Chapter 2 presents a least squares based solution to the LQR based control problem for the DN. The DN network is represented by linear active and passive elements. Given the optimal voltage and current set points for the current operating point of the DN, this algorithm seeks the set of actuation voltages (DER inverter output voltages) which results in stable operating point transfer. Moreover a study on trade-off between sparsity of communication network layer and closed loop stability of the DN is also performed. This chapter also presents a DP based solution for the LQR and discusses a method to curb the oscillation in bus voltages.

Chapter 3 develops the finite horizon OCP subjected to voltage constraints. A network reduction technique is applied to improve the scalability of the algorithm for large scale (MW scale) networks and a novel method is proposed to decouple the problem spatially and temporarily. Comparison studies and various DN case studies are conducted on practical DNs to showcase the effectiveness of the proposed control algorithm.

Chapter 4 presents the contribution of this thesis to the existing state-of-the-art and possible extensions to this work.

Chapter 2

Optimal control of DN via Linear Quadratic Regulator (LQR)

Due to the increased integration of DERs, the current DN is rapidly undergoing changes in the source and load side. These two ends are now dictated by power electronic based converters such as inverters on the source side (Solar PV based DERs) and rectifiers on the load side (for DC loads such as EVs). Thus the DN consists of hundreds of nodes with fast varying power injections and absorptions. These recent changes in the DN have challenged the existing state-of-the-art techniques utilised for V/f control in the DNs. Unfortunately the structure of the DN is not expected to change at a pace to counter these changes. As such the current DN requires efficient and scalable strategies to overcome these issues.

This section formulates the OCP for the DN as an LQR which is subjected to the full scale dynamics of the system. These dynamic equations capture the fast changing nature of the loads and sources in the DN. Perturbations in the DN (source and load) are captured by alternating R, L, and C values used to construct the mathematical model of the DN. In this chapter, we present two analytical approaches employed to solve the optimal LQR problem formulated for the DN.

2.1 Solving LQR via least squares algorithm

This section investigates on solving the OCP for the DN by employing notion of least squares. In this chapter the OCP is formulated as a LQR, which is widely know in control literature [14].

The objective of LQR control is to provide stable set point tracking with minimal control effort (minimum required actuation). Generally the LQR problem is solved via dynamic programming which results in a centralised controller. The least squares solution to the LQR entails in a sparse gain matrix which we leverage to restrict information exchanges between DER agents within a close proximity. Thus the algorithm is scalable to large scale DNs.

2.1.1 Physical Elements

The DN utilised to formulate the OCP is illustrated in Fig. 2.1 which is adopted from reference [14]. The whole network is assumed to be serial interconnection of n subsystems as depicted in Fig. 2.1. Each subsystem consists of a DER unit rated at 0.6 kV and 1.6 MVA, a DER bus, a load connected to the bus and distribution line connecting the subsystems. DER is represented by a 1.5 kV DC voltage source which is coupled to the 13.8 kV DER bus via a low pass filter. This low pass filter consists of a serially connected inductor and resistor whose parameters are designed to restrict the penetration of higher order harmonic signals into the distribution feeder. Loads are designed as a combination of three parallel branches. Purely resistive branch represents heating loads such as incandescent lights, toasters, ovens, space heater etc. Dynamic loads, such as induction motors are represented by a series combination of an inductor a resistor. Local power factor correction equipments are represented by a purely capacitive branch. For the simplicity of this study we only consider linear loads.

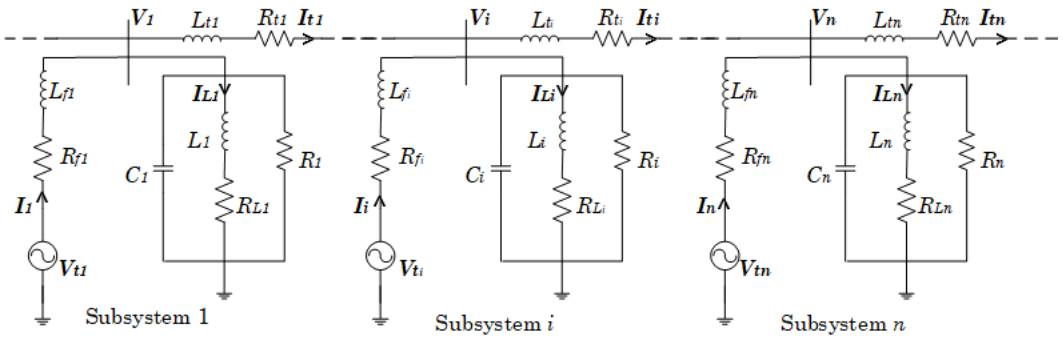

Figure 2.1: Oneline diagram of the DN [1]

Each subsystem consists of five states: bus voltage V_i, DER terminal voltage V_{ti}, DER current I_i, load current in the LR branch I_{Li} and line current I_{ti}, $\forall \in \{1, .., n\}$. The objective of the OCP is to

compute the set of V_{ti},$\forall \in \{1,..,n\}$ which will transfer the system states from one operating point to another smoothly. When a perturbation is sensed in the system (ie,change in load/source) the computed set points (V_{ti}) will be applied to the DER converter terminals. Applying kirchhoff's voltage and current laws to the ith subsystem results in following three phase equations:

$$\begin{aligned}
\frac{dV_{i,abc}}{dt} &= -\frac{V_{i,abc}}{R_i C_i} + \frac{I_{i,abc}}{C_i} - \frac{I_{Li,abc}}{C_i} - \frac{I_{ti,abc}}{C_i} + \frac{I_{ti-1,abc}}{C_i} \\
\frac{dI_{i,abc}}{dt} &= -\frac{V_{i,abc}}{L_{f,i}} - \frac{R_{f,i}}{L_{f,i}} I_{i,abc} + \frac{V_{ti,abc}}{L_{f,i}} \\
\frac{I_{Li,abc}}{dt} &= \frac{V_{i,abc}}{L_i} - \frac{R_{Li}}{L_i} I_{Li,abc} \\
\frac{dI_{ti,abc}}{dt} &= \frac{V_{i,abc}}{L_{ti}} - \frac{V_{i+1,abc}}{L_{ti}} - \frac{R_{ti}}{L_{ti}} I_{ti,abc}
\end{aligned} \tag{2.1}$$

All quantities appear in eq.2.1 are vectors consisting of sinusoidally varying and non-linear a,b and c phase quantities. This leads to complexities in computing the optimal DER terminal voltages V_{ti}, $\forall \in \{1,..,n\}$. In order to overcome this complexity, Park transformation is applied to convert the non-linear quantities to linear quantities as follows:

$$k_{dq} = \begin{pmatrix} cos(\theta) & cos(\theta - \frac{2}{3}\theta) & cos(\theta + \frac{2}{3}\theta) \\ -sin(\theta) & -sin(\theta - \frac{2}{3}\theta) & -sin(\theta + \frac{2}{3}\theta) \\ \frac{1}{\sqrt{2}} & \frac{1}{\sqrt{2}} & \frac{1}{\sqrt{2}} \end{pmatrix} k_{abc} \tag{2.2}$$

where k_{dq} and k_{abc} are resulting vector consisting dq quantities and vector of abc quantities respectively. A global synchronism mechanism is necessary to generate the reference angle θ in eq.2.2. For this all bus agents are equipped with crystal oscillators which are responsible of generating this reference setting by utilising a time reference signal generated by GPS [13]. Applying this

transformation to eq.2.2 results in following set of linear dq equations:

$$\begin{aligned}
\frac{dV_{i,dq}}{dt} &= -\frac{V_{i,dq}}{R_i C_i} + \begin{bmatrix} 0 & w \\ -w & 0 \end{bmatrix} V_{i,dq} + \frac{I_{i,dq}}{C_i} - \frac{I_{Li,dq}}{C_i} - \frac{I_{ti,dq}}{C_i} + \frac{I_{ti-1,dq}}{C_i} \\
\frac{dI_{i,dq}}{dt} &= -\frac{V_{i,dq}}{L_{f,i}} - \frac{R_{f,i}}{L_{f,i}} I_{i,dq} + \begin{bmatrix} 0 & w \\ -w & 0 \end{bmatrix} I_{i,dq} + \frac{V_{ti,dq}}{L_{f,i}} \\
\frac{I_{Li,dq}}{dt} &= \frac{V_{i,dq}}{L_i} - \frac{R_{Li}}{L_i} I_{Li,dq} + \begin{bmatrix} 0 & w \\ -w & 0 \end{bmatrix} I_{Li,dq} \\
\frac{dI_{ti,abc}}{dt} &= \frac{V_{i,dq}}{L_{ti}} - \frac{V_{i+1,dq}}{L_{ti}} - \frac{R_{ti}}{L_{ti}} I_{ti,dq} + \begin{bmatrix} 0 & w \\ -w & 0 \end{bmatrix} I_{ti,dq}
\end{aligned} \tag{2.3}$$

Similar to eq.2.3, the dynamic equations for the rest of the subsystems can be written and all those equations can be aggregated to form the dynamics of the global system as state space equations as follows:

$$\dot{x}(t) = Ax(t) + Bu(t) \tag{2.4}$$

where $x(t)$ is a vector composed of state variables $(V_1, ..., V_i, I_i, I_{Li}, I_{ti}, ..., I_{tn})^T$, $u(t)$ is the input vector consisting the DER actuation voltages vector $(V_{t1}, .., V_{ti}, .., V_{tn})^T$, $A \in \mathbb{R}^{(8n)\times(8n)}$ is the state matrix composed of the DN parameters (ie, R, L and C values in the DN) and $B \in \mathbb{R}^{(8n)\times(2n)}$ is the input matrix consisting low pass filter parameters of DERs. The variables in eq.2.4 are continuous and requires discretization as the computations are performed in a digital computer and sensor readings are discrete in nature [17]. Thus following Eluer's forward approximation is applied to convert eq.2.4 into set of discrete-time equations:

$$\dot{x(t)} \approx \frac{x(t + \Delta t) - x(t)}{\Delta t} \tag{2.5}$$

where Δt is the sampling time interval of the sensor. Substituting eq.3.7 in eq.2.4 and re-arranging the variables accordingly, yields the following discrete-time equations:

$$x(t + \Delta t) = A_D x(t) + B_D u(t) \tag{2.6}$$

where $A_D = \Delta t A + I_n$, $B_D = \Delta t B$ and I_n is an $n \times n$ identity matrix. The sampling time interval Δt must be selected considering the open loop stability of the plant in eq.2.6 and the rated sampling capacity of the sensor devices deployed in the network. A dynamical system is asymptotically stable only if it is open loop stable [13]. The open loop stability of a discrete system is preserved if the eigenvalues of the discrete time state matrix ($eigs(A_D)$) lie within the unit circle drawn on the s-plane centred at the origin. As depicted in Fig.2.2, when $\Delta t = 0.008\ s$ the system is stable as all the eigenvalues lie within the red coloured unit circle and it becomes unstable when $\Delta t = 0.05\ s$ as some of the eigenvalues lie beyond the unit circle. Thus smaller Δt (in this case $\Delta t \leq 0.008\ s$) translates into better open loop stability of the plant due to the better approximation in eq.3.7. Hence open loop stability of the plant determines the upper limit of Δt. Conversely smaller Δt

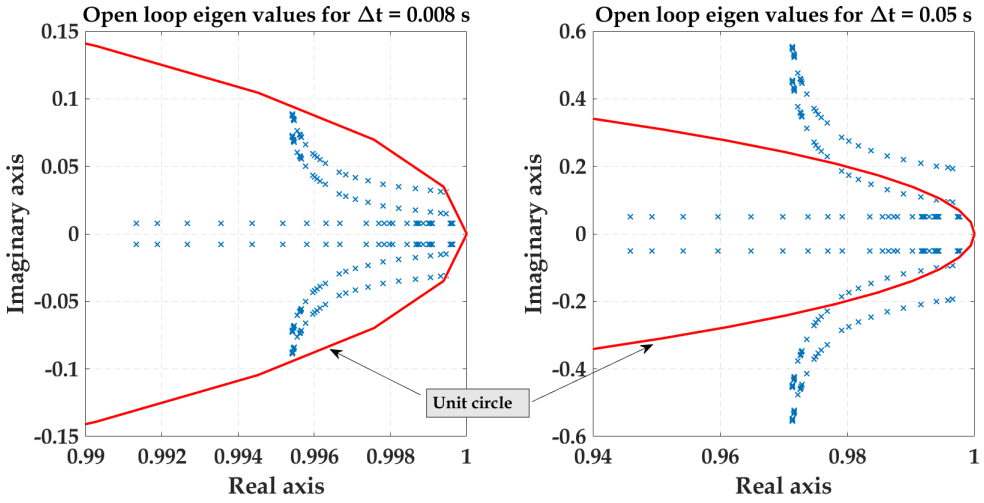

Figure 2.2: Open loop eigenvalues of a 30-bus system for $\Delta t = 0.008s$ (left)and for $\Delta t = 0.05s$(right) [1]

represents higher sampling rate of the sensing devices as,

$$\text{sampling rate} = \frac{1}{\Delta t} \tag{2.7}$$

Therefore, the lower limit of Δt is decided by the sampling capacity of the sensor. For instance micro phasor measurement units allows sampling rates as high as 25000 samples/s ($ie, \Delta t = 400\,\mu s$). Hence for the 30-bus DN the samppling time must lie in between 400 μs and $0.008s$ ($ie, 400\ \mu s \leq \Delta t \leq 0.008\ s$)

2.1.2 Cyber Elements

The modern grid is equipped with intelligent devices called 'bus agents' which are capable of exchanging information with each other and making decisions based on the information received. Each DER bus is equipped with such a bus agent. The communication capabilities of the bus agents in the DN is illustrated in Fig.2.3. In this work we assume a bus agents are capable of 1) exchanging information with other agents; 2) measure local voltages and currents; 3) perform computations. First feature of this bus agent is supported by the modern low power and low cost IEEE wireless communication standards like Zigbee protocol [18]. These devices are reliable and exhibits a typical delay times ranging form 8 ms to 30 ms [14]. This maximum delay time (30 ms) is taken into account while determining the time horizon of the control problem formulated in this chapter and following chapters.

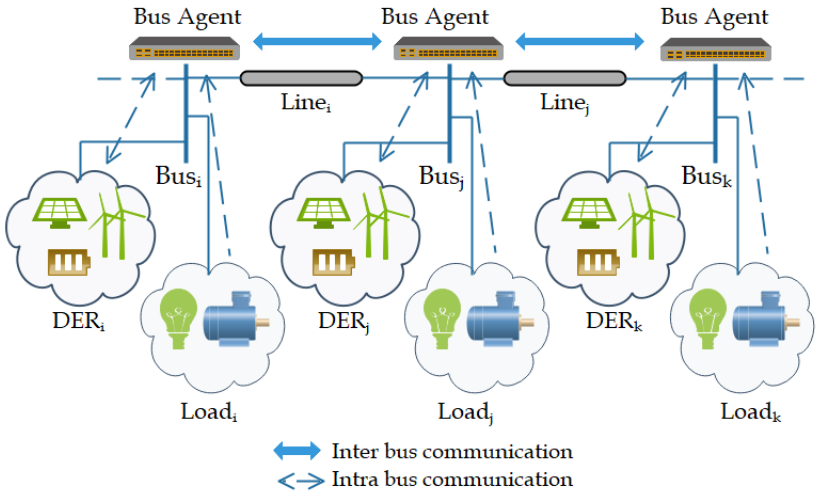

Figure 2.3: Cyber elements of the DN [1]

2.1.3 Finite Horizon LQR

The objective of finite horizon LQR control is to compute the linear actuator $u(t) = K(x_t - x_{ref}(t))$ which minimise the steady state error of the states ($ie,\ x(t) - x_{ref}(t)$) with minimum control effort (minimum control input energy/actuation ($u_{min}(t)$) for a pre-defined finite time period T.

Mathematically this objective can be realised as minimising a separable cost function J_t given below:

$$J_0(x(t), u(t)) = J_0(x(t)) + J_0(u(t)) + J_T \tag{2.8}$$

where $J_0(x(t)) = \sum_{t=0}^{T-1}(x(t) - x_{ref}(t))'Q(x(t) - x_{ref}(t))$ is the cost term which penalises any deviations from the steady state reference, $J_0(u(t)) = \sum_{t=0}^{T-1} u(t)'Ru(t)$ is the cost term which minimises the input actuation, $J_T = x_T'Q_f x_T$ is the term which penalises the states for any deviations in final steady state. $Q \succeq 0$, $R \succeq 0$ and $Q_f \succeq 0$ are state cost matrix, input cost matrix and final state cost matrix respectively. All these matrices are positive semi-definite, which guarantees J_t to be convex (a function is convex if and only if the Hessian of that function is positive semi-definite [19]). The LQR control problem for DNs is usually solved centrally as in references [13, 20] due to the variables coupling between the subsystems. For instance the coupling variables for the ith subsystem are the line current of $(i-1)$th subsystem (I_{ti-1}) and the bus voltage of $(i+1)$th subsystem (V_{i+1}). These variables are also shaded in eq.2.1. In the imminent sections we propose a novel method to strategically decompose the LQR controller problem which restricts the information exchanges within a small neighbourhood of the corresponding subsystem.

2.1.4 Proposed Least Squares Algorithm

The optimal LQR problem for the DN depicted in Fig.2.6 is formulated as follows:

$$P_0: \quad \min_{u(t)} \quad \sum_{t=0}^{T-1}(x(t) - x_{ref}(t))'Q(x(t) - x_{ref}(t)) + \sum_{t=0}^{T-1} u(t)'Ru(t)$$

$$\text{s.t.} \quad \forall t \in \{0, 1..., T-1\}$$

$$x(t + \Delta t) = A_D x(t) + B_D u(t) \quad (C1)$$

where X_{ref} is the state reference vector computed using the steady state power flow algorithm developed in [14]. Constraint $C1$ captures the system dynamics of the DN. Load perturbation are captured by the state matrix A_D as it constitutes of the load parameters R, R_L, L and C as it's elements. When a load change is observed by the bus agent the current state matrix A will be replaced by the perpetuated state matrix $A + \Delta A$, where ΔA captured the load perturbations. B_D is a constant matrix as it constitutes of DER filter parameters. Now, we derive a recursive relation

by manipulating the state space constraint in $C1$.

$$\begin{aligned}
&\text{Substituting } t = 0 \text{ in } C1 \text{ yields :} \\
&x(1) = Ax(0) + Bu(0) \qquad (1) \\
&\text{Substituting } t = 1 \text{ in } C1 \text{ yields :} \\
&x(2) = Ax(1) + Bu(1) \qquad (2) \\
&\text{Substituting } x(1) \text{ in (2) yields :} \\
&x(2) = A^2x(0) + ABu(0) + Bu(1) \qquad (3)
\end{aligned} \tag{2.9}$$

Continuing this recursive process until $t = T - 1$ yields :

$$x(T) = A^T x(0) + A^{T-1}Bu(0) + A^{T-2}Bu(1) + ... + Bu(T-1) \qquad (4)$$

(4) is succinctly experssed as follows :

$$x(T) = A^T x(0) + \sum_{t=0}^{T-1} A^{T-1-j}Bu(j) \quad (5)$$

$\forall t \in \{0, 1..., T-1\}$ these recursive dynamic equitations are written in compact form as follows:

$$\begin{bmatrix} x(0) \\ x(1) \\ x(2) \\ \vdots \\ x(T) \end{bmatrix} = \begin{bmatrix} x(0) \\ Ax(0) + Bu(0) \\ A^2x(0) + ABu(0) + Bu(1) \\ \vdots \\ A^T x(0) + A^{T-1}Bu(0) + A^{T-2}Bu(1) + ... + Bu(T-1) \end{bmatrix} \tag{2.10}$$

eq.2.24 can be succinctly expressed as follows:

$$X = GU + Hx_0 \tag{2.11}$$

where,

$$X = \begin{bmatrix} x(0) \\ x(1) \\ \vdots \\ x(T) \end{bmatrix} \in \mathbb{R}^{(8Tn)}, G = \begin{bmatrix} 0 & 0 & \dots & 0 \\ B & 0 & \dots & 0 \\ AB & B & \dots & 0 \\ \vdots & \vdots & & \\ A^{T-1}B & A^{T-2}B & \dots & 0 \end{bmatrix} \in \mathbb{R}^{(8Tn)\times(2Tn)}$$

$$, U = \begin{bmatrix} u(0) \\ u(1) \\ \vdots \\ u(T-1) \end{bmatrix} \in \mathbb{R}^{(2Tn)}, H = \begin{bmatrix} I \\ A \\ \vdots \\ A^T \end{bmatrix} \in \mathbb{R}^{(8Tn)\times(8n)}$$

X and U in eq.2.11 are vectors formed by concatenation of all the states and inputs from $t = 0$ to $t = T$. Thus this expression captures the system dynamics for a finite time horizon T. This time concatenated dynamics can be used to re-construct the optimal LQR problem as follows:

$$P_{LS} : \min_{U} \quad X' Q_m X + U' R_m U$$

Substituting eq.2.11 for X in P_{LS} yields the following unconstrained least squares objective which is a function of U.

$$P_{LS} : \min_{U} \quad (GU + Hx_0 - r_m)' Q_m (GU + Hx_0 - r_m) + U' R_m U$$

where $r_m \in \mathbb{R}^{(8Tn)}$ is the concatenated steady state reference set points, $Q_m \in \mathbb{R}^{(8Tn)\times(8Tn)}$ and $R_m \in \mathbb{R}^{(2Tn)\times(2Tn)}$ are positive semi-definite matrices of proper dimensions. P_{LS} can be solved analytically by setting the derivative of the objective to 0.

$$\frac{d}{dU}\Big((GU + Hx_0 - r_m)' Q_m (GU + Hx_0 - r_m) + U' R_m U\Big) = 0$$

$$\Rightarrow U = K(r_m - Hx_0), \quad \text{where } K = (G' Q_m G + R_m)^{-1} G' Q_m \text{ is the gain matrix of the controller} \tag{2.12}$$

The eq.2.11 provides the vector U which contains the optimal actuations for a time horizon T. These actuating voltages (V_{ti}, $\forall i \in \{1, ..., n\}$) are utilised as set point terminal voltages for the

DERs which will effectuate the DN voltages and currents to track the optimal steady state reference set points ($x_{ref,i}\,\forall i \in \{1, ..., n\}$) from its initial steady states x_0. The sparsity structure of the gain matrix K determines the information exchanges between DN subsystems in order to achieve this set point tracking. Each non-zero entry in this gain matrix represents a communication link between corresponding subsystem agents. The sparser the gain matrix is, lesser the number of communication links entailed between subsystem agents. Thus the the elements in K should be concentrated toward the diagonal for decentralised communication architecture in the DN. We promote sparsity within this gain matrix K by setting all the elements below a truncating threshold ϵ to eliminate the communication links which are not necessary for the actuating process. The value of ϵ should be selected such that the closed loop stability of plant is preserved.

Next, we present an example case to illustrate the decentralised nature of the controller can be achieved by promoting sparsity within gain matrix K. Fig.2.4 illustrates the sparsity pattern of the gain matrix K for a 30-bus system when $T = 7$ and $\epsilon = 2$. The blue coloured dots represent the non-zero elements of this matrix which are applied to maneuver the system states towards the dynamically changing optimal set points r_m. This set point vector r_m is updated whenever a change ion load/source is observed by the corresponding bus agent. The control action U_1 in the upper triangle of Fig.2.4 represents $Vt1$ and $Vt2$ which are actuating voltages of subsystem 1. Thus the Y-axis of this triangle denote the actuating voltages of subsystems. The X-axis denotes the set of optimal state set points r_m corresponds to each time segment from $T = 1$ to $T = 7$. The actuating voltages are computed based on the expression eq.2.12, which is the product of the entries of the gain matrix and the reference set points. For instance, V_{t1} for time step $T = 7$ is computed by the product of the entries of the first row of the gain matrix K and the set point vector r_m. Thus, the number of entries and its location determines the information exchanges between subsystems. For example, the lower level rectangle depicts the number of subsystems with which the $15th$ subsystem required to communicated to compute the actuating voltages. As colour coded in red, $15th$ subsystem requires set points of 8 sub systems residing in its close proximity. The maximum number of interaction hops for this scenario is 4. The control horizon T is selected heuristically to capture sufficient transient when a perpetuation is observed. Conversely a large T can results in significant computational overheads for the DER agents. Thus selection of T is based on the trade-off between computation complexity of the controller and accuracy.

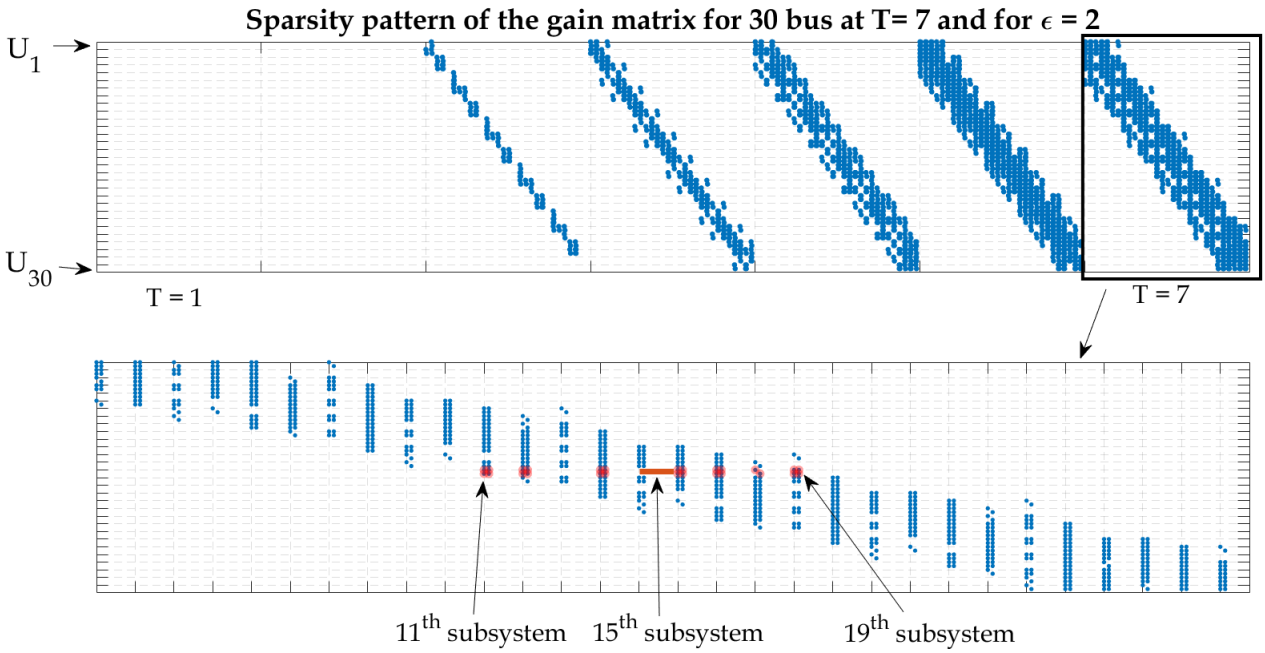

Figure 2.4: Sparsity pattern of gain matrix K when $T = 7$ [1]

2.1.5 Simulation Results

In order to evaluate the defectiveness of the proposed least squares based controller, we simulate the 3-bus DN presented in [13] with the given realistic parameters. For this study we replicate a 30-bus DN by a random series configuration of 30 DER subsystems. Optimal steady state set points (r_m) is computed by utilising the coordination algorithm presented in [14]. All simulations are done in Matlab. We investigate the impact on the voltage stability by the various values taken by the state cost matrix Q_m and the closed loop stability of the system with the communication architecture of the DN.

2.1.5.1 Impact of state cost matrix on the voltage stability

In this study the impact of the state cost matrix on the bus voltage stability of the DN is investigated. The state cost matrix Q_m is constructed by using the positive penalty parameter $\rho > 0$, where $Q_m = \text{Diag}(\rho, \rho..., \rho)$. In order to create the scenario, a load reduction is applied in the DN at $t = 0.016\ s$. The optimal set points are computed by the decentralised techniques states earlier prior to the load change and the algorithm is executed once a change in load/source is observed.

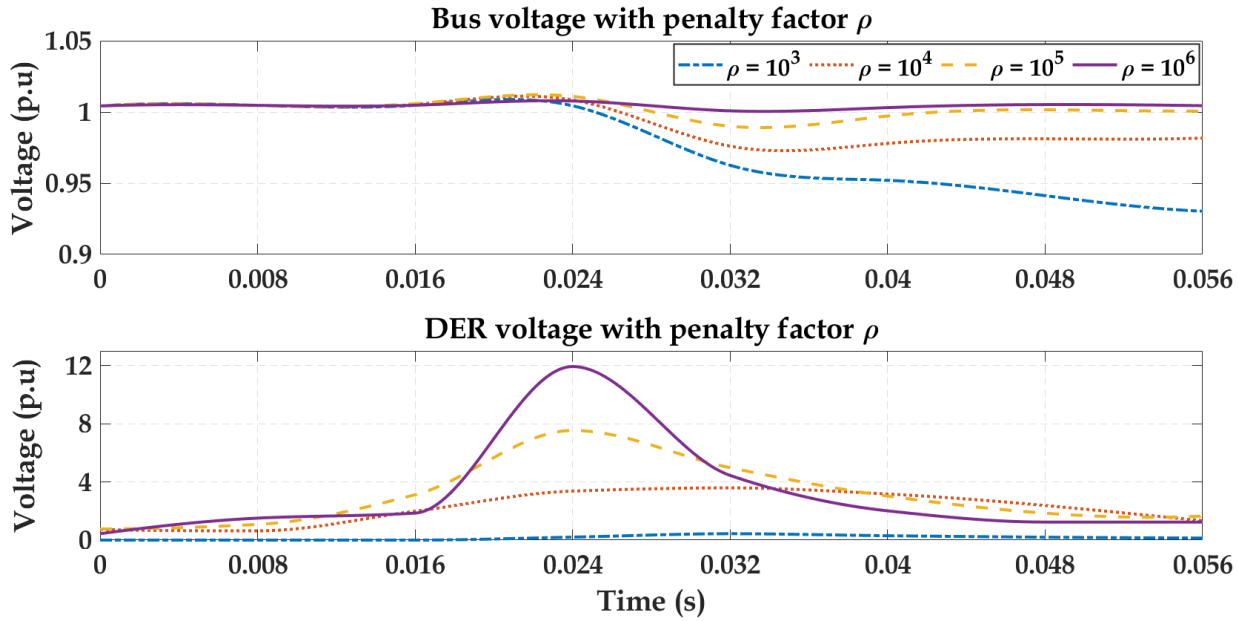

Figure 2.5: Impact of various penalties on the voltage stability [1]

Fig.2.5 shows the variation of bus voltages and DER voltages due to the load disturbance of a randomly selected subsystem residing in the 30-bus DN. Simulations are performed for various penalty parameters ranging from $\rho = 10^3$ to $\rho = 10^6$ and the truncating threshold ϵ is set to a constant value of 2 for all values of ρ. As seen in Fig.2.5, for higher penalty parameters ($\rho = 10^6$) there is virtually no perturbations in the in the bus voltage, hence bus voltage is stable (close to $1p.u$). For lower values of the penalty parameter ($\rho = 10^3$) the voltage tends to be unstable. Conversely, DER voltages take higher values for higher penalty parameters to stabilise the system voltage. This can impose significant stress on the inverter control system of the DER. Hence, the selection of ρ plays a crucial role in the voltage stability of the DN and should be selected considering the trade-off between voltage stability and the inverter output voltage ratings. Most inverters utilised of DER integration purposes have the internal current controlling mechanism to limit its terminal voltage [21].

2.1.5.2 Impact Truncating Threshold on the Closed Loop Stability

In this case study we demonstrate on how to design the communication architecture of the DN while preserving the closed loop stability of the system. The truncating threshold ϵ is heuristically selected by checking the eigenvalues of the closed loop system of the DN. As for the stability of

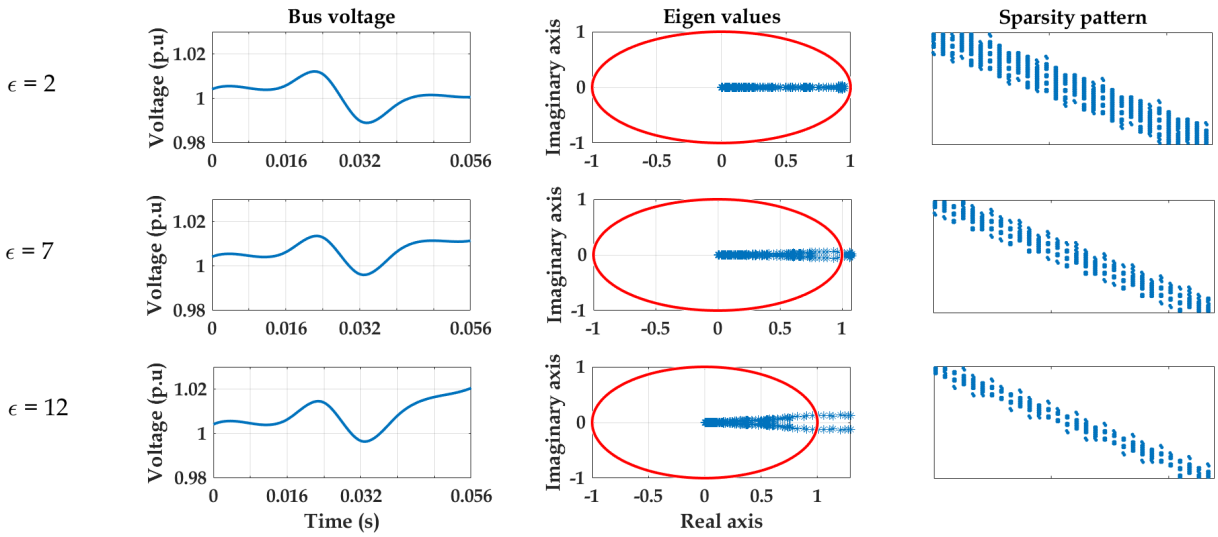

Figure 2.6: Sparsity pattern of gain matrix for $T = 7$ and closed loop stability [1]

discrete system, the closed loop eigenvalues should lie within the unit circle drawn in the s-plane. Fig.2.6 showcases the bus voltage magnitudes, closed loop eigenvalues and the sparsity pattern of the gain matrix K at the time step $T = 7$. For all these scenarios the load reduction is applied at $T = 0.016\ s$. For $\epsilon = 2$ the eigenvalues lie within the red coloured unit circle and the voltage is recovered within two cycles. The communication hops involved in this case for set point exchanges is 4. On the contrary, when ϵ is increased to 12 the communication hops involved in set point exchanges reduce to 2, but some eigenvalues lie beyond the unit circle and the voltage is not recovered. We observed that when ϵ is set to 7 the voltage is marginally stable and eigenvalues lie within the closed unit circle in the s-plane. For this scenario, the number of subsystems involved in communication is 3. Hence the value of ϵ is heuristically selected considering the trade-off between number of communication links and the closed loop stability of the DN.

2.2 Solving LQR via DP

In this section, we solve the optimal LQR problem P_0 by utilising the notion of dynamic programming. The physical system setting and cyber elements are similar to as explained in section 2.1.

2.2.1 Derivation of DP algorithm for the DN

As mentioned in section 2.1.3, the objective of the LQR is to compute the linear regulating actuation $u(t) = K(t)(x(t) - x_{ref}(t))$, that is to compute the gain matrix $K(t)$. In order to elaborate on the DP principle we consider the minimum of the cost function $J_t(x(t), u(t))$,

$$J_t^{min}(x(t), u(t)) = \min_{u(t)} \sum_{t=t}^{T-1} \Big((x(t) - x_{ref}(t))' Q (x(t) - x_{ref}(t)) + u(t)' R u(t) \Big) + x_T' Q_f x_T \tag{2.13}$$

$J_t^{min}(x(t), u(t))$ is the minimum cost that should be incurred by the controller to maneuver the states of the DN from current state $x(t)$ to the desired set points $x_{ref}(t)$. Above expression can be rewritten by separating J_{t+1} from J_t as,

$$\begin{aligned} J_t^{min}(x(t), u(t)) = & \min_{u(t)} \underbrace{(x(t) - x_{ref}(t))' Q (x(t) - x_{ref}(t)) + u(t)' R u(t)}_{\text{current cost (cost at } t = t)} \\ + & \min_{u(t)} \underbrace{\sum_{t=t+1}^{T-1} (x(t) - x_{ref}(t))' Q (x(t) - x_{ref}(t)) + \sum_{t=t+1}^{T-1} u(t)' R u(t) + x_T' Q_f x_T}_{\text{cost-to-go from } t = t+1 (J_{t+1})} \end{aligned} \tag{2.14}$$

From eq.2.14 it is evident that the minimum cost to the controller $J_t^{min}(x(t), u(t))$, depends on current cost incurred and cost to be in incurred starting from $t = t + 1$. Substituting in eq.2.14 for $J_{t+1}^{min}(x(t), u(t))$ yields the following:

$$J_t^{min}(x(t), u(t)) = (x(t) - x_{ref}(t))' Q (x(t) - x_{ref}(t)) + \min_{u(t)} \Big(u(t)' R u(t) + J_{t+1}^{min}(x(t), u(t)) \Big) \tag{2.15}$$

The above cost function $J_{t+1}^{min} > 0$ is quadratic in terms of the states $x(t + \Delta t)$ and can be written as,

$$J_{t+1}^{min}(x(t), u(t)) = (x(t + \Delta t) - x_{ref}(t))' P(t+1) (x(t + \Delta t) - x_{ref}(t)) \tag{2.16}$$

where $P(t+1) \succeq 0$ is a positive semi-definite matrix with appropriate dimensions. The expression for J_{t+1} in eq.2.16 can be substituted in eq.2.15 which results in the following expression:

$$\begin{aligned} J_t^{min}(x(t), u(t)) = \quad & (x_t - x_{ref}(t))' Q (x_t - x_{ref}(t)) + \\ & \min_{u(t)} \Big(u(t)' R u(t) + (x(t+\Delta t) - x_{ref}(t))' P_{t+1} (x(t+\Delta t) - x_{ref}(t)) \Big) \end{aligned} \tag{2.17}$$

In order to find an expression for $x(t+\Delta t)$ in terms of $x(t)$and $u(t)$, we focus on the state space dynamics constraint in P_0. Let's denote the perturbations in states and input from the steady state reference as,

$$\Delta x(t) = x(t) - x_{ref} \quad \text{and} \quad \Delta u(t) = u(t) - u_{ref} \tag{2.18}$$

Substituting expression in eq.2.18 in the state dynamics in P_0 yields the following:

$$\begin{aligned} \Delta x(t+\Delta t) + x_{ref} =& A_D(\Delta x(t) + x_{ref}) + B_D(\Delta u + u_{ref}) \\ \Rightarrow \ \Delta x(t+\Delta t) =& A_D \Delta x(t) + B_D \Delta u + x_{ref} + A_D x_{ref} + B_D u_{ref} \end{aligned} \tag{2.19}$$

The steady state term $x_{ref} + A_D x_{ref} + B_D u_{ref}$ is equal to zero as steady state set points must satisfy the state space dynamics. Thus, the dynamics of the states and input perturbations evolve according to the following expression:

$$x(t+\Delta t) - x_{ref} = \Delta x(t+\Delta t) = A_D \Delta x(t) + B_D \Delta u \tag{2.20}$$

Substituting above dynamics in eq.2.17 yields the following expression for J_t:

$$\begin{aligned} J_t^{min}(x(t), u(t)) = \quad & (x_t - x_{ref}(t))' Q (x_t - x_{ref}(t)) + \\ & \min_{u(t)} \Big(u(t)' R u(t) + (A_D \Delta x(t) + B_D \Delta u)' P_{t+1} (A_D \Delta x(t) + B_D \Delta u) \Big) \end{aligned} \tag{2.21}$$

At minimum cost $J_t^{min}(x(t), u(t))$, the partial derivative of J_t in terms of $u(t)$ must be equal to zero.

$$\frac{\partial}{\partial u(t)} \Big((u(t)' R u(t) + (A_D \Delta x(t) + B_D \Delta u)' P_{t+1} (A_D \Delta x(t) + B_D \Delta u) \Big) = 0 \tag{2.22}$$

This results in following expression for $u(t)$:

$$u(t)^{lqr} = K(t)x(t) + u_{ref}, \text{ where } K(t) = -(R + B_D' P(t+1) B_D)^{-1} B_D P(t+1) A_D \tag{2.23}$$

$u(t)^{lqr}$ is the actuation input voltage set points for the DER inverters which will maneuver current states $x(t)$ to x_{ref} with minimum cost J_t^{min}. The positive semi-definite matrix can be computed by the following recursive expression.

$$P(t) = Q + A' P(t+1) A - A' P(t+1) B (R + B' P(t+1) B)^{-1} B' P(t+1) A \tag{2.24}$$

A derivation for eq.2.24 is provided in [19]. $P(t)$ can be found recursively, working backward from $t = T$ [19]. A summery of dynamic programming algorithm for the DN is provided as follows:

1. Set $P(T) = Q_f$
2. For $t = 0, ...T-1$, compute $P(t)$ using the recursive equation eq.2.24.
3. For $t = 0, ...T-1$, compute the gain matrix $K(t)$ given by eq.2.23.
4. For $t = 0, ...T-1$, compute the optimal actuating input voltages, $u(t)^{lqr}$.

2.2.2 Results

A six bus distribution network which is introduced in reference [2] is selected to validate the presented DP algorithm. Fig.3.3 shows the single line diagram of the six bus network. Nominal voltage is 220 V and nominal frequency is 50 Hz. Base voltage and base power are 220 V and 10 kVA, respectively. The parameters of the six bus network are listed in Table 3.1. Z_1 and Z_2 represent loads which are purely resistive. First, the active power outputs for all 3 DERs are specified to be 4 kW, 5.5 kW and 5 kW for DG1, DG2 and DG3, respectively. These power demands stem from purely resistive loads Z_1 and Z_2. Next, the steady state voltage and current set points ($ie, x_{ref} and\, u_{ref}$) are computed using the power flow equations. A disturbance is applied to the system at $t = 0.05\, s$ by reducing the both resistive loads from $7\,\Omega$ to $6\,\Omega$. After the disturbance, the power set points to be dispatched from the DERs are specified to be 5 kW, 8 kW and 5 kW for DG1, DG2 and DG3, respectively. These power set points are determined based on the available DG capacity and

a market signal. The new DN system set points are computed using the power flow equations. The bus voltage magnitude set points are chosen to be a value between ±5% of the nominal voltage according to IEEE 1547 standards. .

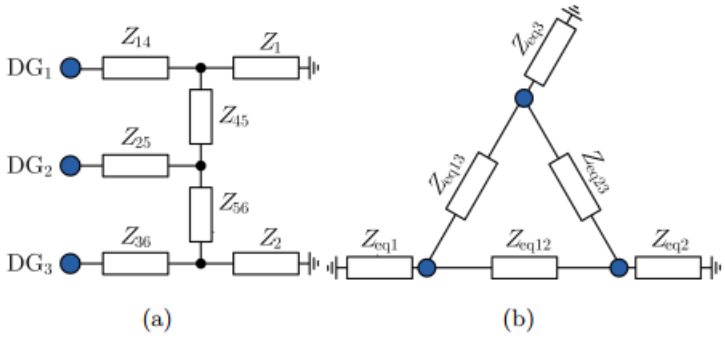

Figure 2.7: One-line diagram of six bus distribution network with 3 DERs [2].

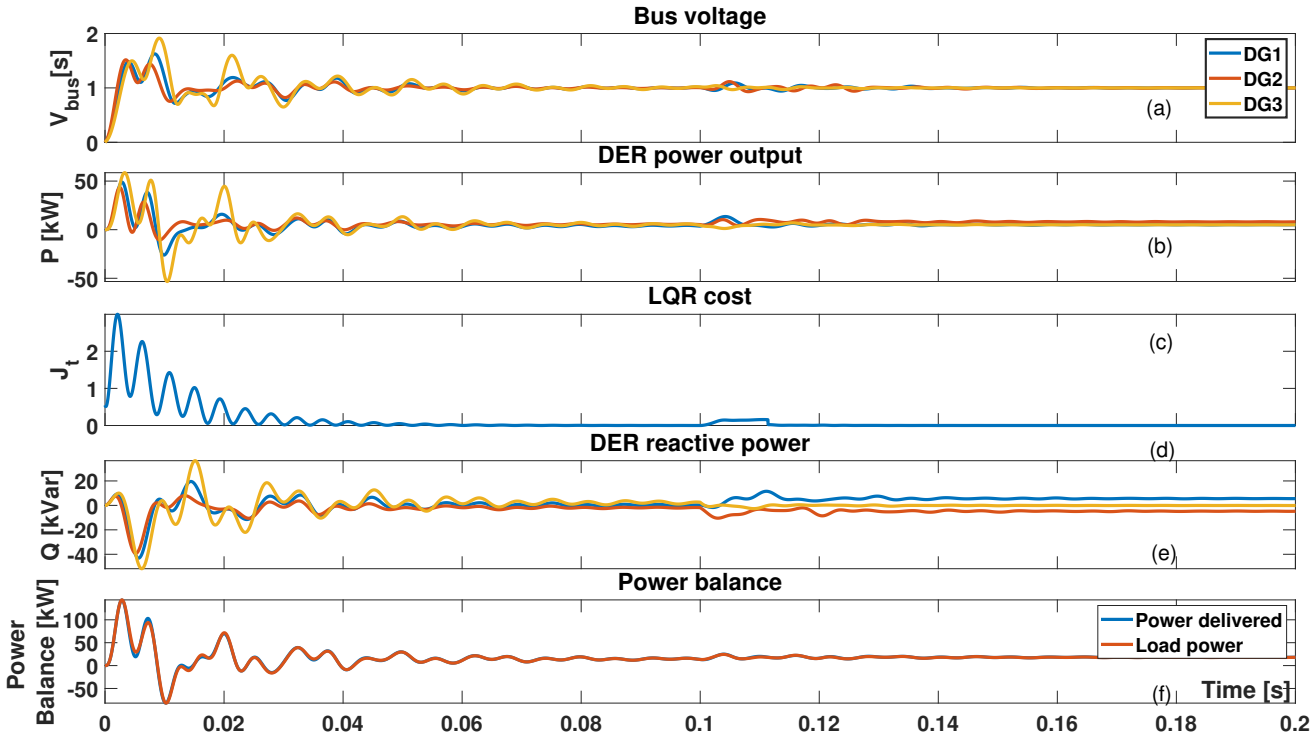

Figure 2.8: Simulations results with low state penalty, (a) bus voltage magnitudes (b) DER active power outputs (c) LQR objective function (d) DER reactive power output (e) load power consumed and (f) total power balance

In order to demonstrate the effectiveness of the DP algorithm, we conduct simulation for two scenarios. Fig. 2.8 shows the simulation results when the penalty matrix (Q) is chosen to be $Q = 0.05\text{diag}(1, 1..., 1, 1)$. As seen in the figure oscillations in the voltage and power signals during

Parameter	Value Ω	Parameter	Value Ω
Z_{14}	$0.03 + \mathbf{j}0.11$	Z_{25}	$0.03 + \mathbf{j}0.11$
Z_{36}	$0.03 + \mathbf{j}0.11$	Z_{45}	$0.23 + \mathbf{j}0.1$
Z_{56}	$0.03 + \mathbf{j}0.58$	Z_1	7
Z_2	7		

Table 2.1: Network parameters of the six bus system

the initial cold start and load change is significant and exceed the system limits. For instance, the cold start transients in the bus voltages and DER active power enduring until 0.08 s. For the second scenario, we increase the penalties on the states and choose the state penalty matrix to be $Q = 10\text{diag}(1, 1..., 1, 1)$. As depicted in Fig. 2.9 the oscillations on voltage and power signals are significantly curbed. As expected, all DER bus voltages in Fig. 2.9(a) are maintained close to 1 p.u throughout the time horizon. Predefined active power set points for all DERs are accurately tracked by the LQR controller as depicted in Fig. 2.9(b). This validates the effectiveness of the algorithm in tracking the reference set points x_{ref} and u_{ref}. This is further validated by the decreasing LQR cost J_t with time plotted in Fig. 2.9(c). The sum of reactive power outputs is zero as seen in 2.9(d) as the DN consists only of purely resistive loads. Finally the balance between DER active power supplied and power consumed by the loads is illustrated in Fig. 2.9(e). This validates the feasibility of the state space constraint of problem P_0.

2.3 Summary

This section proposed two analytical methods to solve the optimal LQR problem formulated for a DN. Given the steady state voltage and current operating points of the DN, the LQR provide tracking of these set points with minimum input and state cost/energy. We have leveraged on the sparsity of the gain matrix to design the architecture of the communication network for information exchange in the DN. It is validated by conducting simulations on practical DN, that this algorithm is effective in tracking desired set points with minimal information exchange within the subsystem agents. The potential of DP algorithm in solving the LQR is also investigated via simulation studies on 6-bus DN. Simulation results showcase the superior ability of the algorithm in set point tracking while maintaining the power balance in the DN and curtailing the oscillations in DER bus voltages.

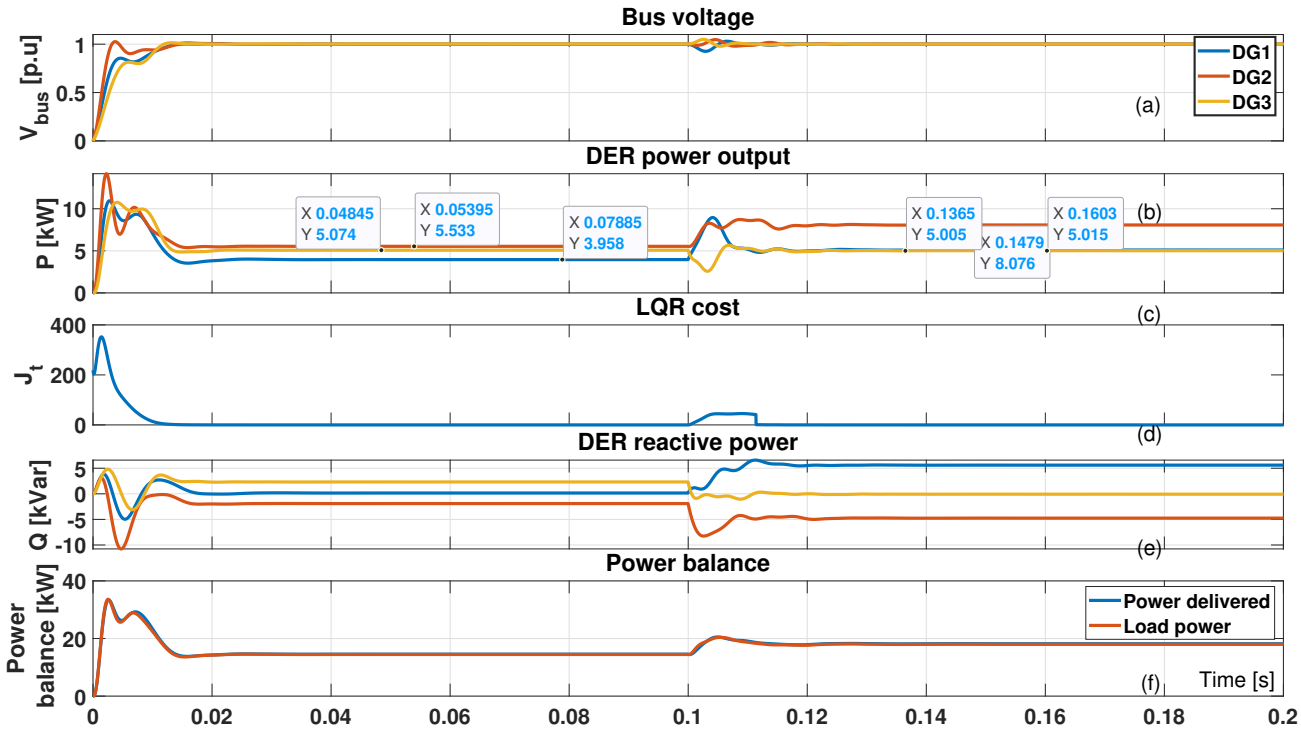

Figure 2.9: Simulations results with high state penalty, (a) bus voltage magnitudes (b) DER active power outputs (c) LQR objective function (d) DER reactive power output (e) load power consumed and (f) total power balance

Chapter 3

Optimal control via S-procedure

Chapter 2 formulated the optimal control problem for DN as a LQR, which tracks the given optimal set points when there is a perturbation in the system. The objective of the LQR is to achieve stable set point transfer with minimum oscillations in states and inputs. The LQR problem does not include economical optimality conditions such as minimising the overall cost of power, minimising the system losses in the distribution lines etc. Moreover the least squares problem formulation does not include the constrain on voltage magnitude limits according to IEEE 1547 standard. Also, DP based LQR is not scalable for large scale DN system due to communication and computation overheads.

In this chapter, we formulate the economically optimal control problem with constraint on voltage magnitudes. As the R/X ratio is significant in the LV and MV networks, we consider minimising the total system losses in the distribution lines, which will also significantly reduce voltage drops in the lines. The state space equations of the electrical equivalent of the DN is included as constraints in the problem. These dynamic equations capture the fast changing nature of the loads and sources in the DN. We use a network reduction technique to physically reduce the DN to a electrically equivalent model which preserves the actuating buses necessary to implement the control algorithm. This network reduction technique enhances the scalability of the algorithm as the communication and computational complexity depends only on the number of DERs connected to the DN.

3.1 Physical system setup

The electrical interdependencies of each component in the DN is comprehensively explained in this section. The practical DN, even with a few hundreds of MWs consists hundreds of nodes, in which some are connected to the DERs (here onwards called as inverter buses). All other nodes are connected to loads called as noninverter buses. As the control actuations are performed at the DER buses, it is useful to eliminate the noninverter buses and reduce the DN to a simpler electrically equivalent reduced network. Thus the reduced order smiler network consists only of active elements of the DN.

3.1.1 Electrical Network Reduction

In this chapter, for convenience, we denote vectors in bold letters. Consider the DN under the consideration consisting n inverter buses (ie., buses connected to inverters) and m noninverter/load buses ($n \cup m = \mathcal{N}$). Let, $\boldsymbol{v_n} = (v_1, ..., v_n)^T, \boldsymbol{i_n} = (i_1, ..., i_n)^T$, $\boldsymbol{v_m} = (v_1, ..., v_m)^T$ and $\boldsymbol{i_m} = (i_1, ..., i_m)^T$, where $\boldsymbol{v_n}, \boldsymbol{i_n} \in \mathbb{C}^{n\times 1}$ and $v_i, i_i \in \mathbb{C}, i = 1, ..., n + m$, denote the vectors of inverter bus voltages, DER current injections, load bus voltages and load currents, respectively. Then, the current-balance equations resulting from Kirchhoff's circuit laws are

$$[\boldsymbol{i_n}, \boldsymbol{i_m}]^T = [Y][\boldsymbol{v_n}, \boldsymbol{v_m}]^T \tag{3.1}$$

where, $Y \in \mathbb{C}^{(n+m)\times(n+m)}$ is the admittance matrix of the network.

Kron reduction. The Kron reduction is ubiquitous in circuit theory and related disciplines, which is employed to obtain a lower dimensional electrically equivalent network [22]. Some applications of the Kron reduction in the context of modelling, analysis and control of power systems can be found in [2, 11, 20, 22] and the references therein. For low inertia networks (ie, LV and MV network), sensing and actuation is performed at the buses connected to the inverters. Thus it is useful to eliminate the noninverter buses and to obtain a simplified network from the perceptive of inverter buses.

Expression eq.3.1 can be rewritten in terms of the block matrices of Y as

$$\begin{bmatrix} \boldsymbol{i_n} \\ \boldsymbol{i_m} \end{bmatrix} = \begin{bmatrix} Y_{nn} & Y_{nm} \\ Y_{nm}^T & Y_{mm} \end{bmatrix} \begin{bmatrix} \boldsymbol{v_n} \\ \boldsymbol{v_m} \end{bmatrix} \tag{3.2}$$

Gaussian elimination of noninverter voltages $\boldsymbol{v_m}$ gives the following relation

$$\boldsymbol{i_n} = Y_{red}\boldsymbol{v_n} + Y_{nm}Y_{mm}^{-1}\boldsymbol{i_m} \tag{3.3}$$

where, $Y_{red} = (Y_{nn} - Y_{nm}Y_{mm}^{-1}Y_{nm}^T)$

The network whose admittance matrix is $Y_{red} \in \mathbb{C}^{n\times n}$, is the Kron reduced network. Y_{red} is a square matrix consisting of complex admittances in the DN. It is noteworthy that in eq.3.3, non-singularity of Y_{mm} is a necessary condition for the existence of Y_{red}. For RLC networks with shunt elements, Y_{mm} can become singular. Even in the presence of capacitive shunt elements, it can be shown that Y_{mm} is always block diagonally dominant [23], thus Y_{mm} is always invertible.

Moreover, it is assumed that power consumed by the constant current loads are negligible ($\boldsymbol{i_m} = 0$). This is a common assumption made by researchers on the works related to low and medium voltage active distribution networks [13, 2, 14]. Setting $\boldsymbol{i_n}$ to 0 in eq.3.3 yields the following relation between inverter bus voltages and DER current injections

$$\boldsymbol{i_n} = Y_{red}\boldsymbol{v_n} \tag{3.4}$$

For RLC networks following properties hold for Y_{red}

1. Y_{red} **exist and is unique**. Y_{red} always exist and unique as Y_{mm} is non-singular.

2. **The graph corresponds to** Y_{red} **is complete**. Two nodes i, j are connected by an edge in the graph $\mathcal{G}_{red}$ corresponding to Y_{red} if and only if there is a path between i and j in graph $\mathcal{G}$ corresponding to Y (see [22] for detailed proof). This property holds as there is always a continuous path to each bus from every other bus in the distribution network (*ie.*, there is no isolated portions/regions in the distribution network).

3. $\mathbf{sum}(Y_{red}) = \mathbf{sum}(Y)$. This property translates into equivalence in load power drawn in original network and the reduced network. Power drawn by an impedance load at a bus is given by $|V|^2y^* \in \mathbb{C}$ where, V: bus voltage and y: load admittance. Assuming 1.0 pu

voltage at the inverter buses and load buses, the load power drawn in original network is given by $\sum_{i=1}^{n+m}\sum_{j=1}^{n+m}[y_{ij}^*] = \mathbf{sum}(\overline{Y}) = \mathbf{sum}(Y)^* = \mathbf{sum}(Y_{red})^* \in \mathbb{C}$ where, $Y = (y_{ij})$. Thus, algebraic summation of elements of Y is equal to $\mathbf{sum}(Y_{red})^*$, which is the load power drawn in the Kron reduced network.

Next the electrical attributes of the Kron reduced network (corresponding to Y_{red}) are explained. Fig. 3.1 depicts the single-line Kron reduced equivalent network of a active distribution network consisting n DERs. In this case Y_{red} will be an $n \times n$ matrix. As shown in the Fig. 3.1, Kron reduced network consists of $\frac{n(n-1)}{2}$ equivalent impedances interconnecting all inverter buses and each subsystem consists of the corresponding DER, its equivalent load and the distribution lines connected to the respective bus. The diagonal elements of Y_{red} represent the equivalent loads at each node and the non-diagonal elements correspond to the distribution line segment between the nodes.

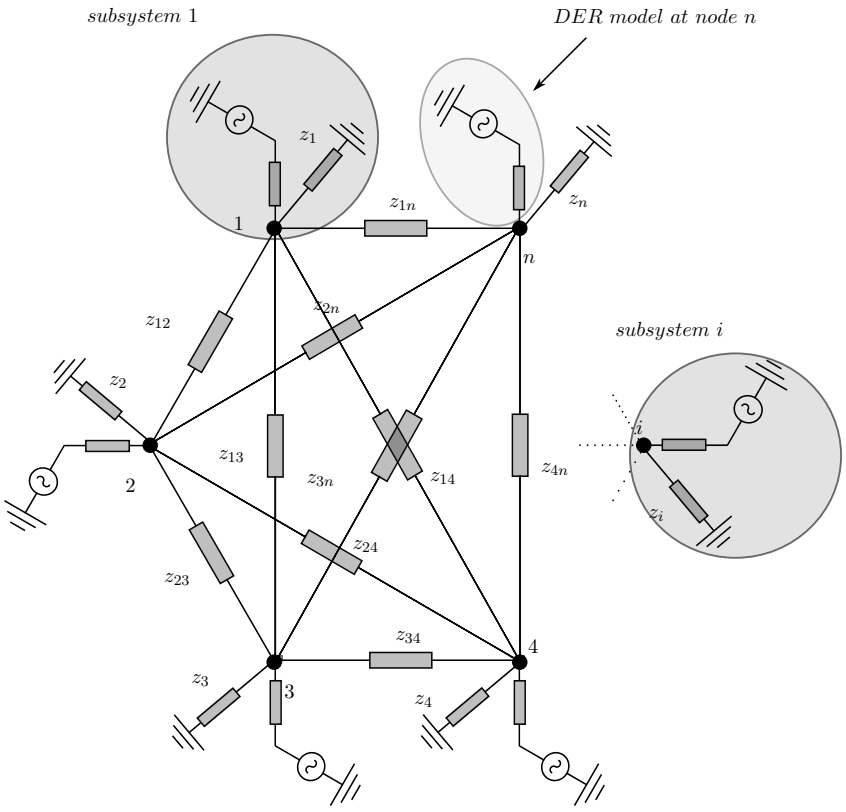

z_i – *Equivalent load at node i.*

z_{ij} – *Equivalent imdepance of distribution line* (i, j).

Figure 3.1: Kron reduced equivalent network of a system consisting n inverter buses [3].

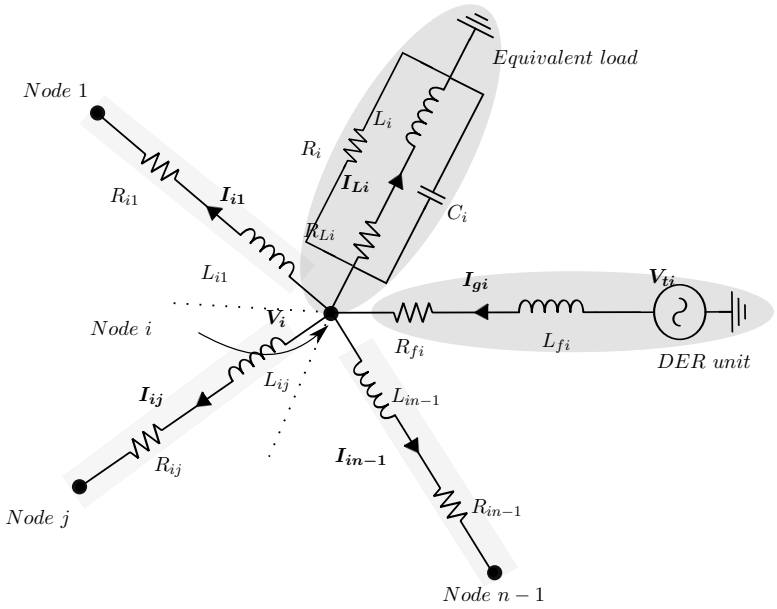

Figure 3.2: Single-line equivalent circuit of ith subsystem [3].

Fig. 3.2: illustrates the single-line per phase electrical equivalent circuit of ith subsystem. All subsystems are assumed to be balanced three phase networks. Although this assumption is not realistic for LV networks, it is an acceptable approximation for MV grids as outlined in reference [24]. DERs are integrated to DN via power electronic converters and are represented by VSC which are connected to the generator buses via low pass filters. Each distribution line is approximated to be series connection of a resistor and an inductor. For load models, lighting and heating equipments are approximated to pure resistors, steady states of dynamic loads such as fans, motors etc are represented by series resistors and inductors and local power factor correction equipment of bulk domestic consumers are purely capacitive [13]. The composite load model is represented by parallel branches of those 3 load components.

State space model. Each subsystem is associated with $n+1$ state variables which are bus voltage V_i, DER current I_{gi}, current drawn by the LC load component I_{Li}, and line current I_{ij} where, $j \in \mathcal{N}_i$) and one input variable (V_{ti}). All these quantities are vectors consisting of three phase components (a, b and c) with each of them synchronously rotating at a frequency of ω. Park's transformation is applied to convert three phase abc quantities to $dq0$ (direct-quadrature-zero) frame of reference quantities. This transformation is ubiquitous in control of power systems literature [13, 8, 25, 9, 14]. Applying Kirchhoff's circuit laws and direct-quadrature-zero transformation to ith subsystem yields

the following state space equations:

$$
\begin{aligned}
\frac{dV_{i,dq}}{dt} &= \begin{bmatrix} 0 & w \\ -w & 0 \end{bmatrix} V_{i,dq} + \frac{I_{gi,dq}}{C_i} - \frac{I_{Li,dq}}{C_i} - \sum_{j \in \mathcal{N}_i} \frac{I_{ij,dq}}{C_i} \\
\frac{dI_{gi,dq}}{dt} &= \begin{bmatrix} 0 & w \\ -w & 0 \end{bmatrix} I_{gi,dq} - \frac{V_{i,dq}}{L_{fi}} - \frac{R_{fi}}{L_{fi}} I_{gi,dq} + \frac{V_{ti,dq}}{L_{fi}} \\
\frac{dI_{Li,dq}}{dt} &= \begin{bmatrix} 0 & w \\ -w & 0 \end{bmatrix} I_{Li,dq} + \frac{V_{i,dq}}{L_i} - \frac{R_i}{L_i} I_{Li,dq} \\
\frac{dI_{i1,dq}}{dt} &= \begin{bmatrix} 0 & w \\ -w & 0 \end{bmatrix} I_{i1,dq} + \frac{V_{i,dq}}{L_{i1}} - \frac{R_{i1}}{L_{i1}} I_{Li1,dq} - \frac{V_{1,dq}}{L_{i1}} \\
&\vdots \qquad\qquad \vdots \\
\frac{dI_{iN,dq}}{dt} &= \begin{bmatrix} 0 & w \\ -w & 0 \end{bmatrix} I_{iN,dq} + \frac{V_{i,dq}}{L_{iN}} - \frac{R_{iN}}{L_{iN}} I_{LiN,dq} - \frac{V_{N,dq}}{L_{iN}}
\end{aligned}
\tag{3.5}
$$

For each variable ($\boldsymbol{x}_{dq} \in \mathbb{R}^2$) dq subscript is affixed to denote the components associated with d and q axes. The dq space time equations in eq.3.5 can be expressed in a compact form as follows :

$$
\dot{\boldsymbol{x}}_i = A_i \boldsymbol{x}_i(t) + \sum_{\forall j \in \mathcal{N}_i} A_j \boldsymbol{x}_j(t) + B_i \boldsymbol{u}_i(t) \tag{3.6}
$$

where, $\boldsymbol{x}_i = (V_{i,dq}, I_{gi,dq}, I_{Li,dq}, I_{ij,dq})^T \quad \forall j \in \mathcal{N}_i$ and $\boldsymbol{u}_i = (V_{ti})^T$. The term $\sum_{\forall j \in \mathcal{N}_i} A_j \boldsymbol{x}_j(t)$ represents all the coupling variables corresponds to neighbouring subsystems which are highlighted in eq.3.5. Hence, the state space model of the global plant (plant consisting n such subsystems) can be expressed as:

$$
\dot{\boldsymbol{x}'} = A\boldsymbol{x}' + B\boldsymbol{u}' \tag{3.7}
$$

where, state vector: $\boldsymbol{x}' = (\boldsymbol{x}_1 ..., \boldsymbol{x}_n)^T$, state matrix: A, input vector: $\boldsymbol{u}' = (\boldsymbol{u}_1 ..., \boldsymbol{u}_n)^T$ and input matrix: B. Since the sensor measurements are obtained at discrete time instances $t_n (ie.,$ at $t_1, t_2 ..)$ and the controller is implemented in a digital computer, linear continuous time relations in eq.3.7 are converted to discrete time equations given by [17]

$$\dot{\boldsymbol{x}'} \approx \frac{\boldsymbol{x}'(t+\Delta t) - \boldsymbol{x}'(t)}{\Delta t} \tag{3.8}$$

Applying the above approximation to eq.3.7 results in the following discrete time state space model

$$\boldsymbol{x}'(t+\Delta t) = A_D \boldsymbol{x}'(t) + B_D \boldsymbol{u}'(t) \tag{3.9}$$

Where, $A_D = \Delta t(A + I_n)$, $B_D = \Delta t B$ and I_n is the n dimensional identity matrix. The sampling time Δt of the PMU units in eq.3.7 should be selected considering the following factors:

1. *open loop stability of the plant* : A dynamic system is asymptotically stable only if it is open loop stable [13]. Selecting a large Δt can result in unstable poles in the closed loop system. This is ensured by fine tuning Δt such that the eigenvalues of A_D lie within the unit circle drawn centred at the origin on the $s-$plane ($\lambda_{max}^M \leq 1$).

2. *sampling capacity of the PMU* : although smaller Δt provides better approximation in eq.3.7, PMUs should have the sufficient sampling capacity ($f = 1/\Delta t$) to measure the voltages and currents. Modern ultra accurate microPMUs guarantee a sampling rate of 25000 samples/s ($or \Delta t = 400\mu s$) [26].

3.2 Cyber elements

We adopt a cyber model for the network where each inverter bus consists of a *bus agent* [18]. In this work, we assume that *bus agents* are capable of 1) exchanging information with neighbouring agents 2) measuring local voltages and currents 3) making intelligent decisions based on the received information and 4) performing a short term load forecast. For the 136-bus Brazilian test feeder network, in which the proposed algorithm will be implemented, bus agents will communicate with neighbouring buses every 80 ms (this is essentially the sampling time Δt). Modern low cost and low power wireless communication standards such as *Zigbee* can deliver reliable information transfer between buses with a delay between 8 ms to 30 ms [14].

3.3 Formulation of finite horizon optimal control problem

Following objectives are defined for the intended optimal control of the distribution network :

- *Providing fast transient response to the perturbations in the system by strategically changing the DER voltage:* Due to the absence of the inertial response to counter the perturbations in loads/sources, LV and MV active distribution networks are prone to V/f fluctuations. This will degrade the power quality supplied to the loads and even damage the sensitive loads (for example, power electronic based loads).

- *Regulating the steady state bus voltage within* $\pm 5\%$ *interval of the nominal voltage:* For the safe and reliable operation of loads, specially for critical loads such as power electronic loads, induction motors etc, voltage should be regulated within this bound specified by revised IEEE 1547 regulation for DER interconnection [27].

- *Supplying the variable active and reactive power demand:* Power demand should be met to avoid unintended load shedding and overloading (which can lead to temporary V/f collapse) in the DN.

- *Maintaining the thermal losses* (aka, i^2r *loss*) *at the global minimum:* Thermal losses in medium and low voltage distribution network are generally significant due to the higher R/X ratio of the distribution lines [28]. Total system losses will be chosen as the objective of the control problem and this objective will be a convex function. This will results in the optimal system states (voltages and currents) with minimum thermal losses at that operating point of the DN.

Following finite horizon optimal control problem is formulated as an optimisation problem for the ith subsystem in $\mathcal{P}_C$ to achieve the objectives outlined above:

$$\mathcal{P}_C: \quad \min_{\boldsymbol{x_i}(t),\boldsymbol{u_i}(t)} \quad \sum_{t=0}^{T}\sum_{i=1}^{n} \boldsymbol{x_i}(t)^T M \boldsymbol{x_i}(t) R_{ij}$$

subject to: $\forall\, i \in \{1, 2...n\}, \forall\, t \in \{1, 2...T\}$

$$\boldsymbol{x_i}(t+1) = A_i \boldsymbol{x_i}(t) + \sum_{\forall j \in \mathcal{N}_i}^{n} A_j \boldsymbol{x_j}(t) + B_i \boldsymbol{u_i}(t) \qquad (C1)$$

$$\beta_i u(t)_i = 0 \ (\beta_i = 1 \ if \ insuffiecient \ DER \ generation, \ otherwise \ \beta_i = 0) \qquad (C2)$$

$$0.95^2 \leq \boldsymbol{x_i}(t)^T Q \boldsymbol{x_i}(t) \leq 1.05^2 \qquad (C3)$$

where $\boldsymbol{x_i}(t) = (V_{i,dq}, I_{gi,dq}, I_{Li,dq}, I_{ij,dq})^T, \boldsymbol{u_i}(t) = (V_{ti,dq}(t))^T,$

R_{ij} – resistance of distribution line ij, $M = \text{Diag}(0, ..., 0, 1, ..., 1)$, and $Q = \text{Diag}(1, 1, 0, .., 0)$.

Constraint $(C1)$ consists of following discrete time space state equations:

$$V_{i,dq}(t+1) = \begin{bmatrix} 0 & w+1 \\ -(w-1) & 0 \end{bmatrix} \Delta t V_{i,dq}(t) + \frac{\Delta t I_{gi,dq}(t)}{C_i} - \frac{\Delta t I_{Li,dq}(t)}{C_i} - \sum_{j \in \mathcal{N}_i} \frac{\Delta t I_{ij,dq}(t)}{C_i} \qquad (c_1)$$

$$I_{gi,dq}(t+1) = \begin{bmatrix} 0 & w+1 \\ -(w-1) & 0 \end{bmatrix} \Delta t I_{gi,dq}(t) - \frac{\Delta t V_{i,dq}(t)}{L_{fi}} - \frac{\Delta t R_{fi}}{L_{fi}} I_{gi,dq}(t) + \frac{\Delta t V_{ti,dq}(t)}{L_{fi}} \qquad (c_2)$$

$$I_{Li,dq}(t+1) = \begin{bmatrix} 0 & w+1 \\ -(w-1) & 0 \end{bmatrix} \Delta t I_{Li,dq}(t) + \frac{\Delta t V_{i,dq}(t)}{L_i} - \frac{\Delta t R_i}{L_i} I_{Li,dq}(t) \qquad (c_3)$$

$$I_{i1,dq}(t+1) = \begin{bmatrix} 0 & w+1 \\ -(w-1) & 0 \end{bmatrix} \Delta t I_{i1,dq}(t) + \frac{\Delta t V_{i,dq}(t)}{L_{i1}} - \frac{\Delta t R_{i1}}{L_{i1}} I_{Li1,dq}(t) - \frac{\Delta t\, V_{1,dq}(t)}{L_{i1}} \qquad (c_4)$$

$$\vdots \qquad \vdots$$

$$I_{iN,dq}(t+1) = \begin{bmatrix} 0 & w+1 \\ -(w-1) & 0 \end{bmatrix} I_{iN,dq}(t) + \frac{\Delta t V_{i,dq}(t)}{L_{iN}} - \frac{\Delta t R_{iN}}{L_{iN}} \Delta t I_{LiN,dq}(t) - \frac{\Delta t\, V_{N,dq}(t)}{L_{iN}} \qquad (c_{n+3})$$

The objective of control problem $\mathcal{P}_C$ is essentially i^2r losses occurring in the distribution lines of the DN over the control horizon T. This objective is convex as the it is a quadratic function of the line currents I_{tij} and the matrix M is positive semi-definite. Constraint $C1$ represents the space-time couplings between the subsystems. A_D^i and B_D^i are discrete state and input matrices of subsystem i. A_D^j captures the space-time physical interactions of subsystem i with neighbouring subsystems. The

second constraint captures the stochastic nature of the ith DER. This is a situation when Solar PV panels are covered by clouds or wind turbines are stalled due to insufficient wind speed. Intended DER disconnection due to a fault or routine maintenances will also be captured by this constraint. The final constraint $C3$ guarantees voltage magnitude to be regulated within $\pm 5\%$ interval of the nominal voltage as outlined in the revised version of IEEE 1547 DER interconnection regulation. The time taken to compute the control actuations is approximately $0.01 * T + C$, where C is the time taken to solve the problem $\mathcal{P}_C$. In the next section we conclude that C is equals to 50 s with proper justifications. We observe following challenges in solving $\mathcal{P}_C$ by each bus agent :

- The control problem $\mathcal{P}_C$ for each subsystem is formulated as an optimisation problem with constraint. This cannot be solved using analytical methods. A proper iterative technique should be chosen considering global convergence, time taken to solve the problem and optimality of the solution
- In constraint $C1$, the coupling variable $\boldsymbol{x_i}(t+1)$, belongs to $(t+1)$th time step and the variable summation, $\sum_{\forall j \in \mathcal{N}_i}^{n} A_j \boldsymbol{x_j}(t)$ belongs to neighbouring subsystems. Independent and simultaneous computations cannot be performed by each bus agent at a specific time step in the presence of these couplings.
- The bus voltage lower limit ($0.95^2 \leq x_i(t)^T Q x_i(t)$) in $C3$ is a non-convex set as $\boldsymbol{x_i}(t)$ does not satisfy the definition of convex sets [19]. Solving non-convex problems is at least NP-hard which translates into intractability of the problem [14].

These difficulties in solving $\mathcal{P}_C$ are tackled by utilising a novel variable separable technique and exact convex relaxations using S-procedure and Schur's compliment which are discussed in the following section.

3.4 Proposed Finite Horizon Optimal Control Algorithm

In this section we propose a highly granular and scalable control algorithm to solve the constrained control problem $\mathcal{P}_C$. The optimal control problem $\mathcal{P}_C$ is executed for a time horizon T whenever a perturbation in load/source is predicted by the agents. Then the resulting set of optimal VSC terminal voltage set points (magnitude and angle of $V_{ti}, \forall i \in \mathcal{N}_i$) are communicated by each agents

to its respective VSC control system to generate corresponding Pulse Width Modulation (PWM) signals.

The notion of perceptive variables is exploited in this paper to decompose $\mathcal{P}_C$ to subproblems which can be solved by each bus agent. The concept of perspective variables was originally introduced in [16] to solve the optimal OPF in distribution networks. The OCP differs significantly from OPF as 1) the system constraints in OCP are differential equations while in OPF those are algebraic equations and 2) establishment of perspective variables for both spatial and temporal couplings to decompose the global problem into subproblems.

The distributed solver ADMM is used to solve the subproblems associated with each agents. The application of ADMM allows to transform the non convex constrain to an exact convex relaxation using Schur's compliment and S-procedure [14]. This convex transformation and the application of ADMM guarantee feasibility and linear convergence of original problem $\mathcal{P}_C$.

3.4.1 Problem decomposition

Decomposition of problem $\mathcal{P}_C$ for each bus agent i for the time instance t (henceforth denoted as subsystem agent (i,t)) is not straightforward due to the presence of spatial and temporal coupling variables in constraints $(c_1)-(c_{n+3})$. These constraints contain spatial coupling variables such as V_1 in c_4, and V_n in c_{n+3}. These variables belong subsystem agents $(1,t)$ and (n,t) respectively. As of temporal coupling, constraints $(c_1)-(c_{n+2})$ contain variables belong to agent $(i,t+1)$ $(ie, V_i(t+1), I_{gi}(t+1)\ etc)$ on the left hand side of the equations. In order to overcome this issue, subsystem agent (i,t) will maintain two sets of variables namely, 1) set of local variables $x_i(t)$ and 2) set of perspective variables $y_i(t)$. All the states that belong to subsystem agent (i,t) form the set of local variables $x_i(t)$:

$$x_i(t) = \{V_i(t), I_{gi}(t), I_{Li}(t), \{I_{ij}(t)|\text{for some } j \in \mathcal{N}_i\}, V_{ti}(t)\} \tag{3.10}$$

All the feasible points defined by non-convex bus voltage lower bound constrain $(C3)$ form the set $\mathcal{X}_i(t)$. The local variables in $x_i(t)$ should satisfy this bus voltage lower bound constrain, thus $x_i(t) \subseteq \mathcal{X}_i(t)$. Perspective variables are estimates of local and coupling variables. All the perspective

variables belong to subsystem agent (i,t) form the set $y_i(t)$:

$$
\begin{aligned}
y_i(t) &= \{\text{perspectives of } a \in x_{i,t}\} \cup \{\text{perspectives of } a \\
&\quad \in x_{i,t+1}\} \cup \{\text{perspectives of } a \in x_{j,t} | \text{for some } j \in \mathcal{N}_i\} \\
&\quad = y_{(i,i)}(t,t) \cup y_{i,i}(t+1,t) \cup y_{j,i}(t,t) \\
&\quad = \{V_{i,i}(t,t), I_{gi,i}(t,t), I_{Li,i}(t,t), \{I_{ij,i}(t,t)| \\
&\quad \text{for some } j \in \mathcal{N}_i\}, \\
&\quad V_{ti,i}(t,t)\} \cup \{V_{i,i}(t+1,t), I_{gi,i}(t+1,t), I_{Li,i}(t+1,t), \\
&\quad \{I_{ij,i}(t+1,t) | j \in \mathcal{N}_i\}\} \cup \{V_{j,i}(t,t), I_{ji,i}(t,t)| \\
&\quad \text{for some } j \in \mathcal{N}_i\}
\end{aligned}
\tag{3.11}
$$

The subscripts of perspective variables contain two indices corresponding to physical subsystems and two entries inside the pair of round brackets corresponding to time instances. First index in subscript and first entry in the brackets denote the perspective of and second index in subscript and second entry in the brackets denote the perspective from. For instance, $V_{i,i}(t+1,t)$ denotes the bus voltage of subsystem agent $(i,t+1)$ from the perspective of subsystem agent (i,t). All feasible points defined by convex constraints (constrains except for the bus voltage lower bound) in $\mathcal{P}_C$ form the set $\mathcal{Y}_i(t)$. Perspective variables should satisfy these constrains, thus $y_i(t) \subseteq \mathcal{Y}_i(t)$.

Now, the global problem $\mathcal{P}_C$ is spatially and temporarily decomposable for each subsystem agent (i,t). However, this collection of subproblems solved by bus agents will not be equivalent to $\mathcal{P}_C$ unless perspective variables are equal to its corresponding local variables. Hence, consensus must be established between perspective variables $y_i(t)$ and local variables $x_i(t)$, $x_i(t+1)$ and $x_j(t)$. Problem $\mathcal{P}_C$ is reformulated in $\mathcal{P}'_C$ along with the consensus constraints:

$$\mathcal{P}'_C: \quad \underset{x_i(t),y_i(t)}{\text{minimize}} \sum_{t=0}^{T}\sum_{i=1}^{n}\sum_{j\in\mathcal{N}_i}(I_{ij}^{(x)}(t))^2 R_{ij}$$

subject to : $\forall\, i \in \{1,2...n\}, \forall\, t \in \{1,2...T\}$,

$$x_i(t) \subseteq \mathcal{X}_i(t) \qquad (C1')$$

$$y_i(t) \subseteq \mathcal{Y}_i(t) \qquad (C2')$$

$$[V_i(t)^{(x)} = V_{i,i}(t,t)^{(y)},\ I_{gi}(t)^{(x)} = I_{gi,i}(t,t)^{(y)},$$
$$I_{Li}(t)^{(x)} = I_{Li,i}(t,t)^{(y)},\ I_{ij}(t)^{(x)} = I_{ij,i}(t,t)^{(y)},$$
$$V_{ti}(t)^{(x)} = V_{ti,i}(t,t)^{(y)}] \text{ for some } j \in \mathcal{N}_i \qquad (C3)'$$
$$[V_i(t+1)^{(x)} = V_{i,i}(t+1,t)^{(y)},$$
$$I_{gi}(t+1)^{(x)} = I_{gi,i}(t+1,t)^{(y)},$$
$$I_{Li}(t+1)^{(x)} = I_{Li,i}(t+1,t)^{(y)},$$
$$I_{ij}(t+1)^{(x)} = I_{ij,i}(t+1,t)^{(y)}] \text{ for some } j \in \mathcal{N}_i \qquad (C4)'$$
$$[V_j(t)^{(x)} = V_{j,i}(t,t)^{(y)},$$
$$I_{ji}(t)^{(x)} = I_{ji,i}(t,t)^{(y)}] \text{ for some } j \in \mathcal{N}_i \qquad (C5)'$$

The Lagrangian function $\mathcal{L}_\rho$ associated with $\mathcal{P}'_C$ is as follows

$$\mathcal{L}_\rho(x,y,\lambda) = f(x) + \lambda(x-y) + \frac{\rho}{2} \parallel x-y \parallel_2^2 \quad \text{where} \quad f(x) = \sum_{t=0}^{T}\sum_{i=1}^{n}\sum_{j\in\mathcal{N}_i}(I_{ij}(t))^2 R_{ij} \qquad (3.12)$$

$$\lambda(x-y) = \sum_{t=0}^{T}\sum_{i=1}^{n}\Bigg(\lambda_i(t)(x_i(t) - y_{(i,i)}(t,t)) + \lambda_i(t+1)(x_i(t+1) - y_{(i,i)}(t+1,t)) + \sum_{j\in\mathcal{N}_i}\lambda_j(t)(x_j(t) - y_{(j,i)}(t,t))\Bigg) \qquad (3.13)$$

$$\parallel x-y \parallel_2^2 = \sum_{t=0}^{T}\sum_{i=1}^{n}\Bigg(\parallel x_i(t) - y_{(i,i)}(t,t) \parallel_2^2 + \parallel x_i(t+1) - y_{(i,i)}(t+1,t) \parallel_2^2 + \qquad (3.14)$$

$$\sum_{j\in\mathcal{N}_i} \parallel x_j(t) - y_{(j,i)}(t,t) \parallel_2^2 \Bigg) \qquad (3.15)$$

Superscripts (x) and (y) are used to denote variables belong to $x_i(t)$ and $y_i(t)$ respectively. $(C3)'$, $(C4)'$ and $(C5)'$ are the consensus constraints for local variables, temporarily coupled variables and spatially coupled variables respectively. After the addition of these consensus constraints, problems $\mathcal{P}_C$ and $\mathcal{P}'_C$ are equivalent. In order to decompose $\mathcal{P}'_C$ in terms of local and perspective variables using ADMM, augmented Lagrangian $\mathcal{L}_\rho(x, y, \lambda)$ is constructed in (3.12). $\lambda_i(t), \lambda_i(t+1)$ and $\lambda_j(t)$ are the sets dual variables and penalty term $\rho > 0$ imposes strict convexity on $\mathcal{L}_\rho(x, y, \lambda)$ [14]. At the k^{th} iteration of ADMM, each subsystem agent (i, t) sequentially conducts optimisations over $x_i(t)$ and $y_i(t)$ to update local, perspective and dual variables as follows

$$
\begin{aligned}
x_i(t)^k &\in \underset{x_i(t)\subseteq\mathcal{X}_i(t)}{\operatorname{argmin}} \quad \mathcal{L}_\rho(x, y^{k-1}, \lambda^{k-1}) && (L1)\\
y_i(t)^k &\in \underset{y_i(t)\subseteq\mathcal{Y}_i(t)}{\operatorname{argmin}} \quad \mathcal{L}_\rho(x^k, y, \lambda^{k-1}) && (L2)\\
\lambda_i(t)^k &= \lambda_i(t)^{k-1} + \rho(x - y) && (L3)
\end{aligned}
$$

For every iteration k, subsystem agents will simultaneously update variables belong to all time instances $t \in \{1, ...T\}$. All the spatial coupling variables are updated at the current iteration are broadcasted to all other DER bus agents $(ie, \text{for some } j \in \mathcal{N}_i)$ while all the temporal coupling variables are communicated to subsystem agents $(i, t-1)$, and $(i, t+1)$. For instance after the $x_i(t)$ update in $L1$, local variable sets $\{V_i(1), ..., V_i(T)\}$ and $\{I_{ij}(1), ..., I_{ij}(T), \text{for some } j \in \mathcal{N}_i\}$ are broadcasted to all other DER bus agents $i = 1, .., n$ while $x_i(t)$ is send to subsystem agent $(i, t+1)$. This iterative refinement process is repeated until the residual $\| x - y \|_2^2$ falls below the predefined threshold ϵ. When $\| x - y \|_2^2 < \epsilon$, the resulting final values of the variables are the global optimal solutions x_o,y_o and λ_o of problem $\mathcal{P}_C$. However, since the set $\mathcal{X}_i(t)$ is non-convex, the objective $f(x)$ is not guaranteed to converge to the globally optimal solution $f(x_o, y_o, \lambda_o)$.

3.4.2 Resolving the non-convexity

In order to guarantee global convergence of f, an exact convex relaxation technique is proposed by applying Schur's compliment and S-procedure. The generalised form of the local variable subproblem solved by each subsystem agent (i, t) in $x_i(t)$ update step $L1$ of ADMM is constructed as a

quadratically constrained quadratic program ($QCQP$) in $\mathcal{P}_{L1}$ as follows

$$\begin{aligned}
\mathcal{P}_{L1}: \quad & \underset{x_i(t)}{\text{minimize}} \quad x_i(t)^{'}(A_{0i,t}+B_{0i,t})x_i(t)+2C_{0i,t}x_i(t) \\
& \text{subject to :} \\
& x_i(t)^{'}(A_{1i,t})x_i(t)+D_{i,t}\leq 0 \qquad (C6')
\end{aligned}$$

where $A_{0i,t}=\text{diag}(0,0,0,0,0,0,0,0,R_{i1}...R_{ij},0,0)$, for some $j\in\mathcal{N}_i$ is the coefficient pertaining to the objective f and $B_{0i,t}=0.5\text{diag}(\theta_1\rho,\theta_1\rho,\theta_2\rho,\theta_2\rho,\theta_3\rho,\theta_3\rho,\theta_{11}\rho,..,\theta_{1j}\rho,\theta_4\rho,\theta_4\rho)$, for some $j\in\mathcal{N}_i$ is the coefficient corresponds to the augmented terms in $\mathcal{L}_\rho$. $\theta_1,\theta_1,\theta_1$ and θ_{1j} are positive integers whose values depend on the number of DER buses (n) in the network. $C_{0i,t}$ represents remaining linear terms in $\mathcal{L}_\rho$ and $A_{1i,t}=\text{diag}(-1,-1,0,...,0)$ represents the coefficient pertaining to the bus voltage magnitude lower bound constrain. The objective of $\mathcal{P}_{L1}$ is convex as the Hessian of diagonal matrix $(A_{0i,t}+B_{0i,t})$ is positive definite (eigenvalues of a diagonal matrix are essentially the corresponding diagonal elements). The constrain $(C6')$ is non-convex since the Hessian of $A_{1i,t}$ is negative semidefinite (eigenvalues values are $-1,-1$ and zeros). Now, we focus on constructing the dual problem of the non-convex optimisation problem $\mathcal{P}_{L1}$. The Lagrangian function $\mathcal{L}_\mathcal{D}$ of $\mathcal{P}_{L1}$:

$$\begin{aligned}
\mathcal{L}_\mathcal{D} &= x_i(t)^{'}(A_{0i,t}+B_{0i,t})x_i(t)+2C_{0i,t}x_i(t)+\nu(x_i(t)^{'}(A_{1i,t})x_i(t)+D_{i,t}) \\
&= x_i(t)^{'}(A_{0i,t}+B_{0i,t}+\nu A_{1i,t})x_i(t)+2C_{0i,t}x_i(t)+D_{i,t}
\end{aligned} \tag{3.16}$$

ν is the Lagrangian multiplier associated with $(C6)'$. Setting the partial derivative of $\mathcal{L}_\mathcal{D}$ to zero provides a linear relationship between ν and $x_i(t)$ as follows

$$\begin{aligned}
\frac{\partial}{\partial x_i(t)}(x_i(t)^{'}(A_{0i,t}+B_{0i,t}+\nu A_{1i,t})x_i(t)+2C_{0i,t}x_i(t)+D_{i,t})=0 \\
x_i(t)=-(A_{0i,t}+B_{0i,t}+\nu A_{1i,t})^{-1}C_{0i,t}
\end{aligned} \tag{3.17}$$

Substituting this expression for $x_i(t)$ in $\mathcal{L}_\mathcal{D}$ gives the dual objective $g(\nu)$ as follows

$$g(\nu)=\nu D_{i,t}-C_{0i,t}^{'}(A_{0i,t}+B_{0i,t}+\nu A_{1i,t})^{-1}C_{0i,t} \tag{3.18}$$

The dual problem of this non-convex ($QCQP$) is now constructed in $\mathcal{D}_{L1}$

$$\begin{aligned}
&\mathcal{D}_{L1}: \quad \underset{\nu}{\text{maximize}} \quad g(\nu) \\
&\text{subject to :} \\
&\nu \geq 0 && (C7)' \\
&A_{0i,t} + B_{0i,t} + \nu A_{1i,t} \succeq 0 && (C8)'
\end{aligned}$$

where dual objective $g(\nu) = \nu D_{i,t} - C_{0i,t}^T (A_{0i,t} + B_{0i,t} + \nu A_{1i,t})^{-1} C_{0i,t}$, ν is the Lagrangian multiplier associated with $(C6)'$ and $(C8)'$ is necessary to enforce non-trivial solutions on $\mathcal{D}_{L1}$. The concave dual problem of $\mathcal{D}_{L1}$ can be converted to a SDP problem $\mathcal{S}_{L1}$ by applying Schur's compliment as follows [19]:

$$\begin{aligned}
&\mathcal{S}_{L1}: \quad \underset{\nu,\gamma}{\text{maximize}} \quad \gamma \\
&\text{subject to :} \\
&\nu \geq 0 && (C9)' \\
&\begin{bmatrix} (A_{0i,t} + B_{0i,t}) & C_{0i,t} \\ C_{0i,t}^T & -\gamma \end{bmatrix} + \nu \begin{bmatrix} A_{1i,t} & 0 \\ 0 & D_{i,t} \end{bmatrix} \succeq 0 && (C10)'
\end{aligned}$$

$\mathcal{S}_{L1}$ can be solved to to obtain the value of γ at optimality (γ_o). As presented in Theorem 2 in [14], S-procedure states that, strong duality holds between the primal problem $\mathcal{P}_{L1}$ and the dual problem $\mathcal{S}_{L1}$ if primal problem $\mathcal{P}_{L1}$ is the strictly feasible. This convex SDP problem $\mathcal{S}_{L1}$ cane be solved to obtain the value of dual variable ν at optimality (ie, ν_0). Thus, the globally optimal solution of $\mathcal{P}_{L1}(ie, x_o)$ can be recovered by substituting ν_0 back in eq.3.17 ($ie, x_0 = -(A_{0i,t} + B_{0i,t} + \nu_0 A_{1i,t})^{-1} C_{0i,t}$).

3.4.3 Summary of the proposed algorithm

Since both local and perspective variables updates of ADMM are convex minimisation problems, the iterative refinement process listed in algorithm Alg. 1 is guaranteed to converge to the globally optimal solution. This algorithm will be executed when a perturbation in load/source is forecasted.

The resulting set of VSC terminal voltages (magnitudes and angles) will be utilised as set points to dispatch the corresponding DER which will result in minimum total thermal losses in the network.

Algorithm 1 Proposed Algorithm for Subsystem Agent (i,t)

Initialization:
$x_i(t) \leftarrow x_i(t)^0, y_i(t) \leftarrow y_i(t)^0, \lambda_i(t) \leftarrow \lambda_i(t)^0, k \leftarrow 0$ and residual $r^k \leftarrow \infty$
Algorithm:

While $r^{k+1} < \epsilon$
Compute $x_i(t) \leftarrow \underset{x_i(t) \subseteq \mathcal{X}_i(t)}{\operatorname{argmin}} \quad \mathcal{L}_\rho(x, y^k, \lambda^k)$

- Solve $\mathcal{S}_{L1}$ for γ and recover x from $x(A_{0i,t} + B_{0i,t})x = \gamma$
- broadcast $x_i(t)$ to some $\mathcal{N}_i$ and send $x_i(t)$ to agent $(i, t-1)$

$y_i(t) \leftarrow \underset{y_i(t) \subseteq \mathcal{Y}_i(t)}{\operatorname{argmin}} \quad \mathcal{L}_\rho(x^{k+1}, y, \lambda^k)$

- broadcast $y_i(t)$ to some $\mathcal{N}_i$ and send $y_i(t)$ to agent $(i, t+1)$

$\lambda_i(t) \leftarrow \lambda_i(t)^k + \rho(x - y)$

- broadcast $\lambda_i(t)$ to some $\mathcal{N}_i$ and send $\lambda_i(t)$ to agent $(i, t+1)$
- Update residual $r^{k+1} \leftarrow r^k + (x - y)$
- $k \leftarrow k + 1$

End While

3.5 Results

In this section the effectiveness and scalability of the proposed optimal controller is validated by simulations on realistic active distribution networks. All simulations are conducted in PSCAD® and MATLAB® which are installed in a personal computer consisting a 12-core processor with 3.6 GHz speed. We utilise CVX solver and $fmincon$ functions in MATLAB to solve the (x) and (y) problems, respectively.

3.5.1 Equivalency between original network and Kron reduced network

First, the equivalency between original and reduced order DN is validated. As the algorithm, Alg. 1 is implemented for the reduced order DN, it is crucial that the electrical attributes of the DN is preserved during the Kron reduction process. Simulations are conducted in PSCAD software to validate this property of the Kron reduction technique. The six bus distribution network (shown in Fig. 3.3) which is presented in reference [2] is selected to perform this validation. The network

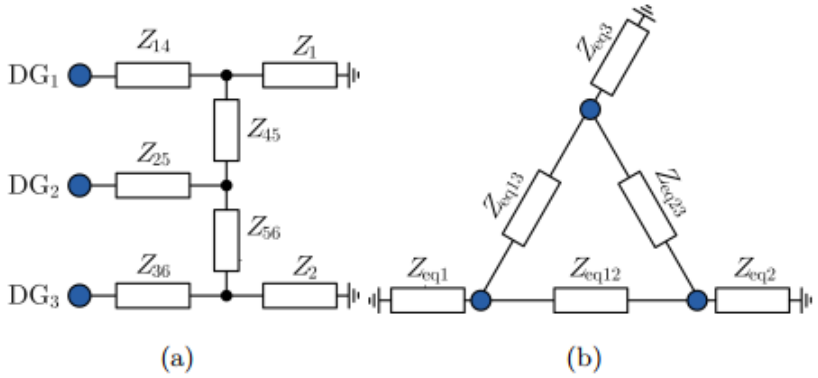

Figure 3.3: Oneline diagram of six bus distribution network with 3 DERs. (a) Original network and (b) Kron reduced network [DERs are represented by blue dots] [2]

parameters of this DN is listed in Table.3.1. Validation is done by observing similar responses (DER power outputs, aggregated load power drawn etc) in both networks when DERs in both networks are actuated by similar input voltages (ie, V_{ti}). For this, DER active power outputs are randomly selected to supply the total load active power demand of 5.1 kW. This load power demand is the power consumed by purely resistive loads Z_1 and Z_2 at the nominal voltage, 220 V. For this case DER active power outputs are randomly selected to be 2.4 kW, 0.5 kW and 2.2 kW for DG1, DG2 and DG3, respectively. Then the set point voltages (V_{ti}) for 3 DERs are computed for the original network using the power flow equations. Then DERs in both networks are actuated with the computed set point voltages V_{ti}. Fig. 3.4(a) and Fig. 3.4(b) depict active power dispatched in original network and Kron reduced network, which are equal to the predefined values for the original network. Fig. 3.4(c) shows the active power consumed by Z_1 and Z_2 at 200 V in original network. Fig. 3.4(c) shows the power consumed by equivalent loads in Kron reduced network. For both cases the aggregated active power consumptions are equal to 5.1 kW. Moreover the line losses in both networks are equal to approximately 20 W as illustrated in Fig. 3.4(c). This attribute of reduced order network is crucial as the objective of the optimal control problem $\mathcal{P}_C$ is the total network losses. These similar responses verify the electrical equivalency of the original network and its Kron reduced network.

Parameter	Value Ω	Parameter	Value Ω
Z_{14}	$0.03 + \mathbf{j}0.11$	Z_{25}	$0.03 + \mathbf{j}0.11$
Z_{36}	$0.03 + \mathbf{j}0.11$	Z_{45}	$0.23 + \mathbf{j}0.1$
Z_{56}	$0.03 + \mathbf{j}0.58$	Z_1	20
Z_2	18		

Table 3.1: Network parameters of the six bus system

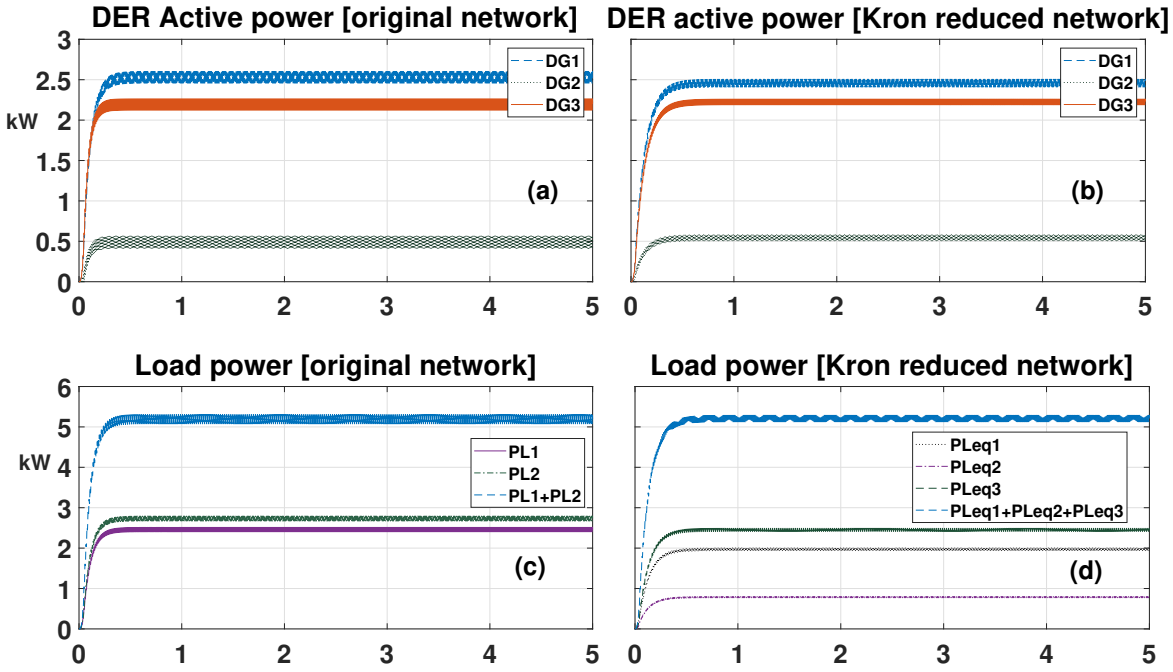

Figure 3.4: Equivalency between original six bus network and Kron reduced network (a) DER active power and (c) load power consumption in original network. (b) DER active power and (d) load power consumption in Kron reduced network

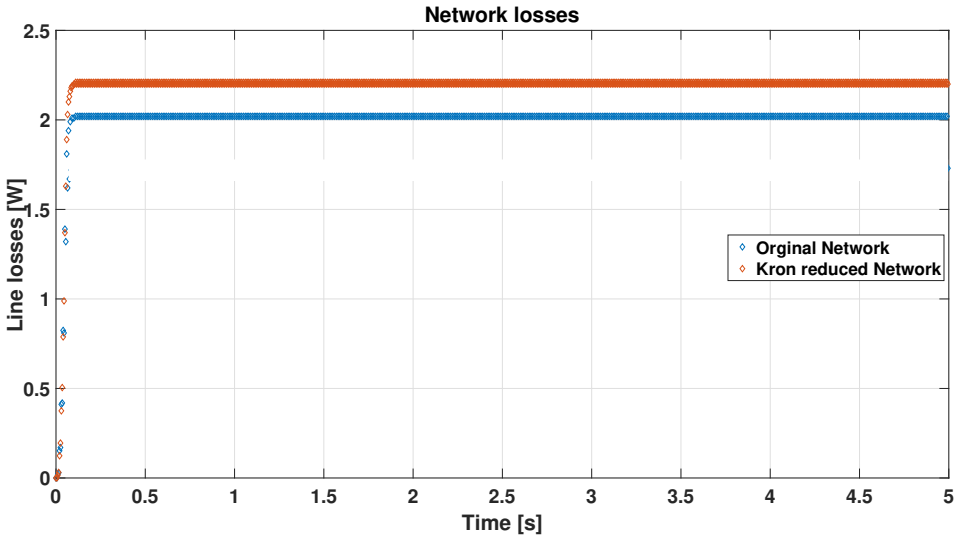

Figure 3.5: Network losses in original network and Kron reduced network

3.5.2 Comparative study

The six bus distribution network which is presented in reference [2] is selected to perform comparison studies. Fig. 3.3 shows the single line diagram of the six bus network. Nominal voltage is 220 V and nominal frequency is 50 Hz. Base voltage and base power are 220 V and 10 kVA, respectively. The parameters of the six bus network are listed in Table 3.1. Z_1 and Z_2 represent loads which are purely resistive. First the proposed optimal control algorithm in Alg. 1 is implemented on the six bus system to solve for optimal DER set points which will results in minimum losses. Then the problem is solved for the final steady state by a centralised solver. A step load change of 484 W is applied at $t = 0.05$s to the network by increasing Z_2 from $18\,\Omega$ to $22\,\Omega$.

Fig. 3.6(a) depicts variation of DER voltages, which settles down to the final steady states within 0.05s. Fig. 3.6(b) shows the decrease in active power from the initial demand of 5.108 kW to the final steady state demand of 4.602 kW. The residual seems to decrease with number of iterations as in Fig. 3.6(c), which showcases the convergence of the algorithm. The global optimal value of the objective value (ie, total loss) is computed using the centralised solver is 3.5239×10^{-14}. This objective value corresponds to the final steady states shown Fig. 3.6(a) and Fig. 3.6(b). As seen in Fig. 3.6(d), the objective value converges to the aforementioned global optimal value after 102 ADMM iterations. Thus, it is evident that centralised performance is achieved by the proposed optimal controller within 102 ADMM iterations.

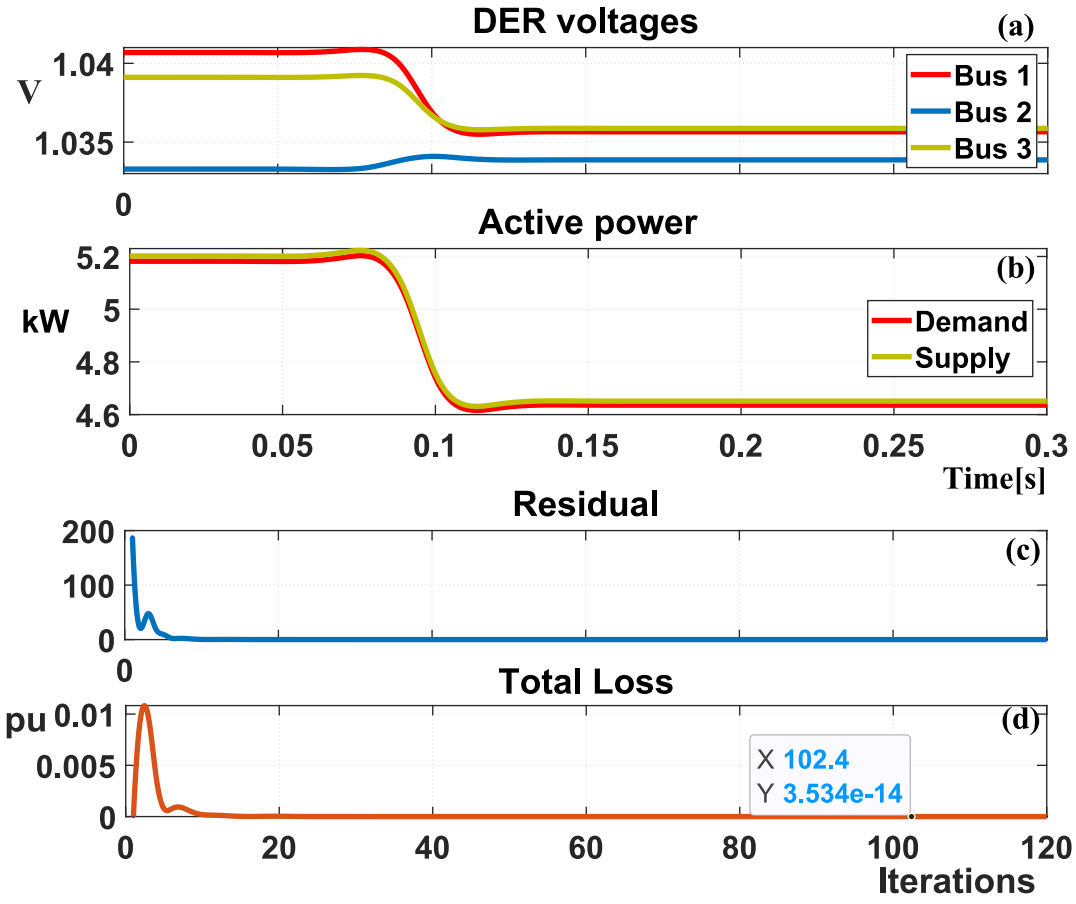

Figure 3.6: (a) DER voltages (b) active power balance (c) residual and (d) objective function value for a step load change in six bus network

3.5.3 Impact of initial conditions on convergence

It is identified that the initial conditions on the ADMM has an effect on the convergence speed of the algorithm. For the case shown in Fig. 3.6(d), the initial conditions are selected randomly. Initial condition for local and perspective variables are set to be matrices of ones and initial condition for dual variable is set to be a matrix of ones. For the case shown in Fig. 3.7, initial conditions of variables are set to be the steady state values of those variables prior to the load change. As seen in Fig. 3.7 the objective function converges to the global optimal value of 3.5239×10^{-14} within around 95 ADMM iterations, which is faster than for the case of random initial conditions described above.

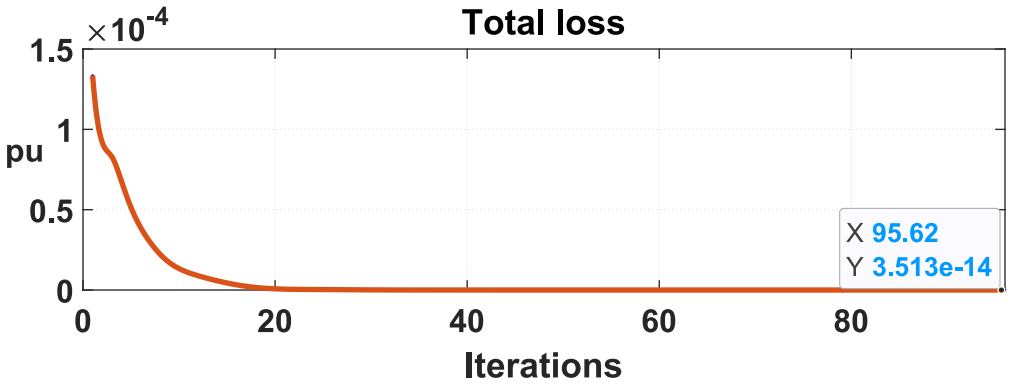

Figure 3.7: Objective function value for fine tuned initial conditions

3.5.4 Case studies on scalability

Fig. 3.8 shows the structure of 136-bus Brazilian distribution network utilised to demonstrate various scenarios that can occur in a distribution network. The two thick long lines denote substation buses and all other thin lines denote the rest of the medium voltage buses in the network.

The active and reactive power loads and parameters of the distribution lines of the network are taken from [29]. The rated bus voltage of the network is 13.8 kV (V_{nom}), nominal frequency is 60 Hz and rated nominal capacity (connected load) is 18.2 MW. Base voltage and base power are chosen to be 13.8 kV and 100 MVA. 10 DERs are connected to the network at buses, 2, 48, 57, 62, 67, 76, 125, 141, 148 and 207. For all the case studies Δt is set to be 0.01s, which is selected based on the open loop stability criteria outlined in section II.

Case study 1: For the first case the system response to a step change in active power load is demonstrated. Active power demand is simultaneously increased at each feeder by 80 kW, which accounts for around 8.5 MW of active power demand in the whole network. This load increment is triggered at $t = 0.05s$. This sudden increase in active power demand should be catered by the 10 DERs according to Alg. 1. Fig. 3.9 depicts bus voltages at buses connected to the DERs ($V_i \; \forall i \in n$), DER voltages ($V_{ti} \; \forall i \in n$) and DER output currents ($I_{gi} \; \forall i \in n$). All theses voltages and currents are smoothly transitioned from one optimal steady state to another steady state within 0.04s of transient period. As seen in Fig. 3.9(a) the bus voltage dynamics are contained within the $\pm\%5$ bound of the nominal voltage ($V_{nom} \pm \%5$). This validates the feasibility of non-linear convex and non-convex bus voltage magnitude constraints in $C3$ of problem $\mathcal{P}_C$. Fig. 3.9(b) illustrates DER voltages which are utilised as VSC set points for the smooth transfer of system states. As in Fig. 3.9(c), all DERs smoothly ramp up the output current to supply the increase in load demand. The value of the object function $f(x_i(t))$(ie, total losses) and the residual of the optimisation problem with respect to the iteration number (k) is depicted in Fig. 3.10(a) and Fig. 3.10(b) respectively. The objective f rapidly decreases and settles down to a value of 0.0022 MW after around 450 ADMM iterations. Similarly the residual which is essentially the gap between local and perceptive variables, rapidly decreases with number of iterations as shown in Fig. 3.10(b). The residual value after 500 ADMM iterations is $1.02 \times 10^{-6} \approx 0$, which means consensus is met between local and perspective variables. Global active power balance between sources and loads is shown in Fig. 3.10(c). The active power demand is met throughout the time horizon and settles at 26.7 MW after the load increase at $t = 0.05s$ from its' initial load demand of 18.2 MW. This validates the feasibility of the dynamic constraints $C1$ of problem $\mathcal{P}_C$.

Case study 2: This case study investigates the performance of the optimal controller to a sudden DER disconnection. This scenario is triggered by disconnecting the DER connected to the bus 207 at $t = 0.05s$. Unintentional DER disconnection can occur due DER circuit breaker operation in an instance of a fault. This scenario also reflects the case where sudden drop in DER power generation due to unexpected variations in atmospheric conditions such as clouds covering Solar Photovoltaic (PV) based large scale power generation units. Fig. 3.11(a) shows bus voltages at buses connected to DERs. Although the sudden disconnection causes voltage fluctuations, these variations are contained within the predefined voltage bandwidth ($V_{nom} \pm \%5$) imposed by the

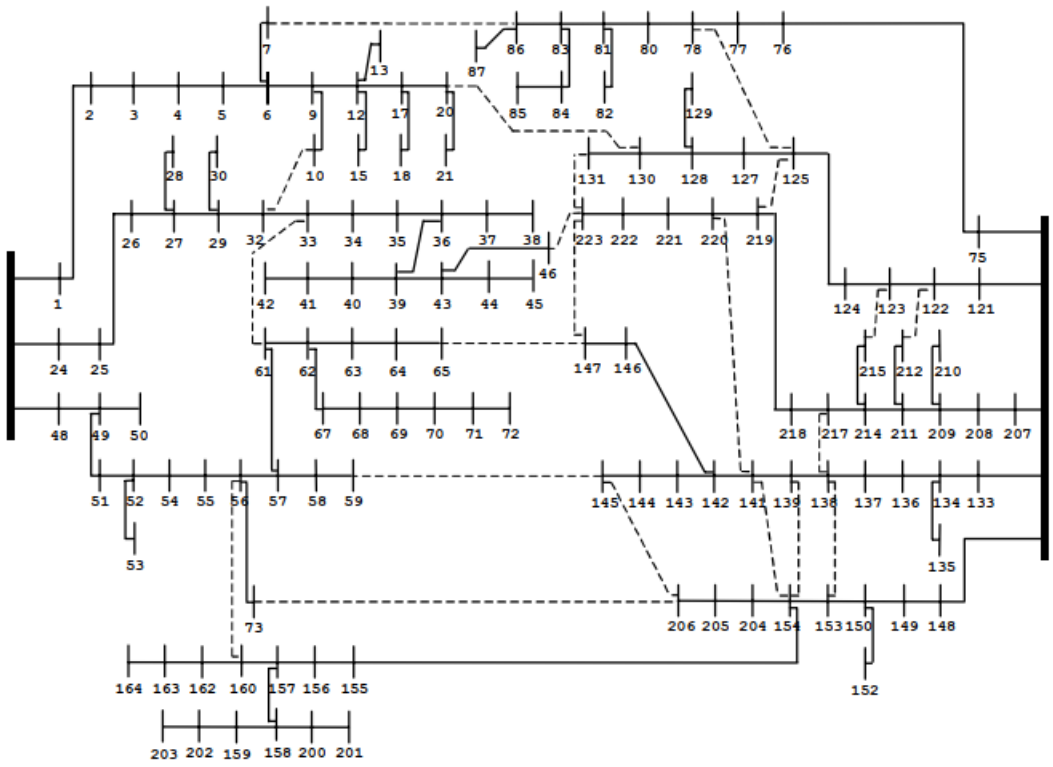

Figure 3.8: 136-Bus Brazilian distribution network

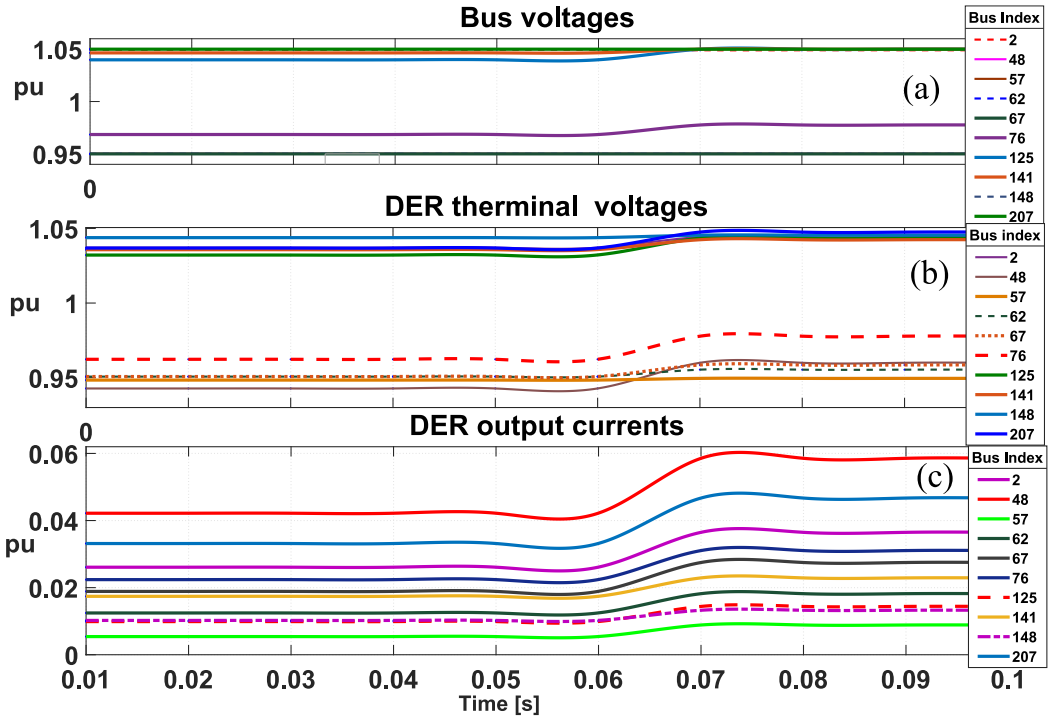

Figure 3.9: Trajectories of (a) bus voltages (b) DER voltages and (c) DER output currents for a step change is active power load for a step load change in Brazilian network

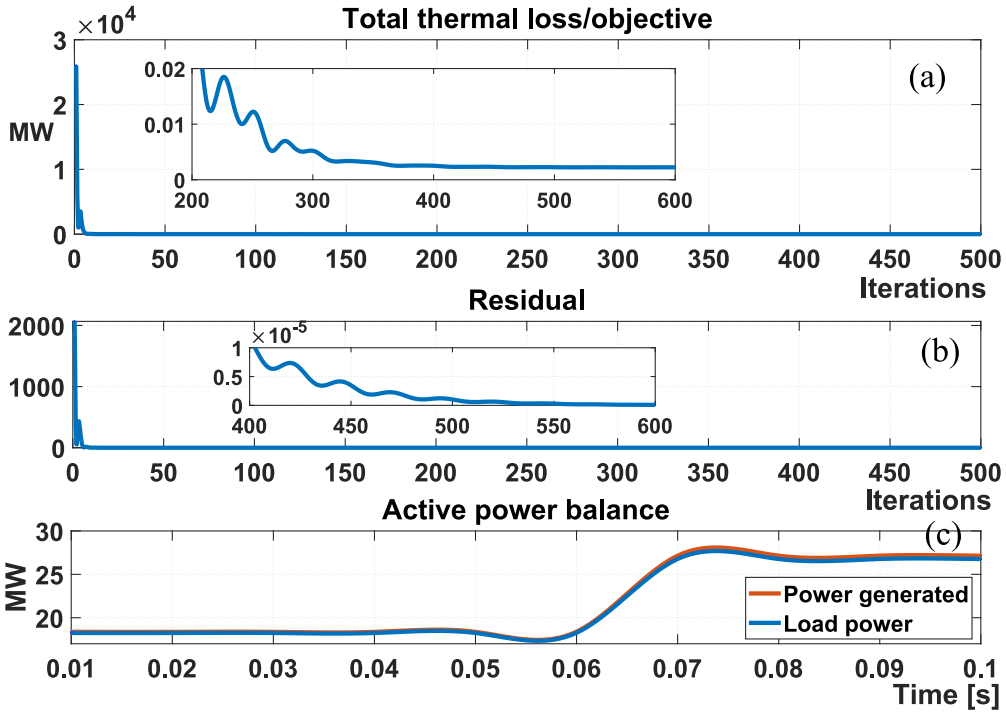

Figure 3.10: (a) Objective function value/losses (b) residual and (c) active power balance for a step load change in Brazilian network

constraints in $C3$. Thus, the power quality is preserved. Fig. 3.11(b) and Fig. 3.11(c) show DER voltages and active power outputs, respectively. Prior to the disturbance, DER at bus 207 delivers an active power of 0.86 MW, which falls to zero after its disconnection at $t = 0.05s$. As depicted in Fig. 3.11(c), remaining DERs ramp up the active power output in order to supply the power deficit of 0.86 MW caused by the DER disconnection. This is further validated as the active power delivered before and after the disconnection are steady at the rated nominal value of 18.2 MW, which is shown in Fig. 3.12(c). Additionally the rapid decrease of objective function value in Fig. 3.12(a) and residual in 3.12(b), showcases the convergence of the algorithm and feasibility of the constraints in $\mathcal{P}'_C$. It takes around 500 iteration for the algorithm to converge to the global optimal solution. Each iteration consists of 3 rounds of information exchanges (local, perspective and dual variables update). Each round of information exchange is assumed to take around 30 ms which is the maximum delay time entitled with existing communication protocol. Based on this assumption it will take 45 s ($500 \times 30 \times 3 = 45,000\ ms$), which is less than a minute to completely execute the algorithm. This time interval requires the agents to forecast changes in supply and demand for 1 minute time horizon. Load fornicating with this low time intervals is subjected to negligible error

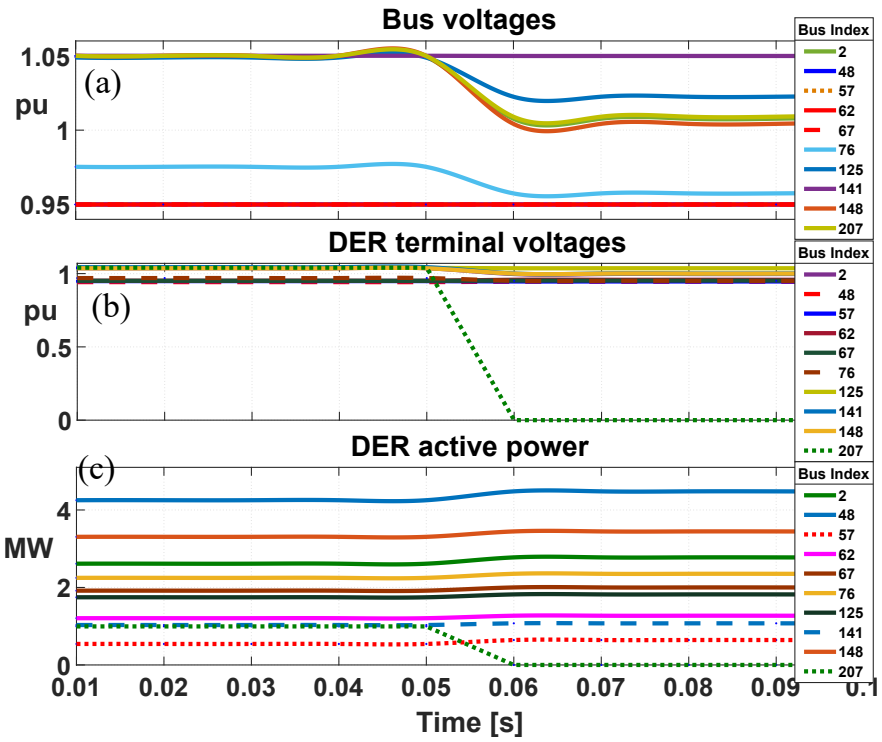

Figure 3.11: (a) Bus voltages (b) DER voltages and (c) DER output currents during sudden DER trip at bus 207

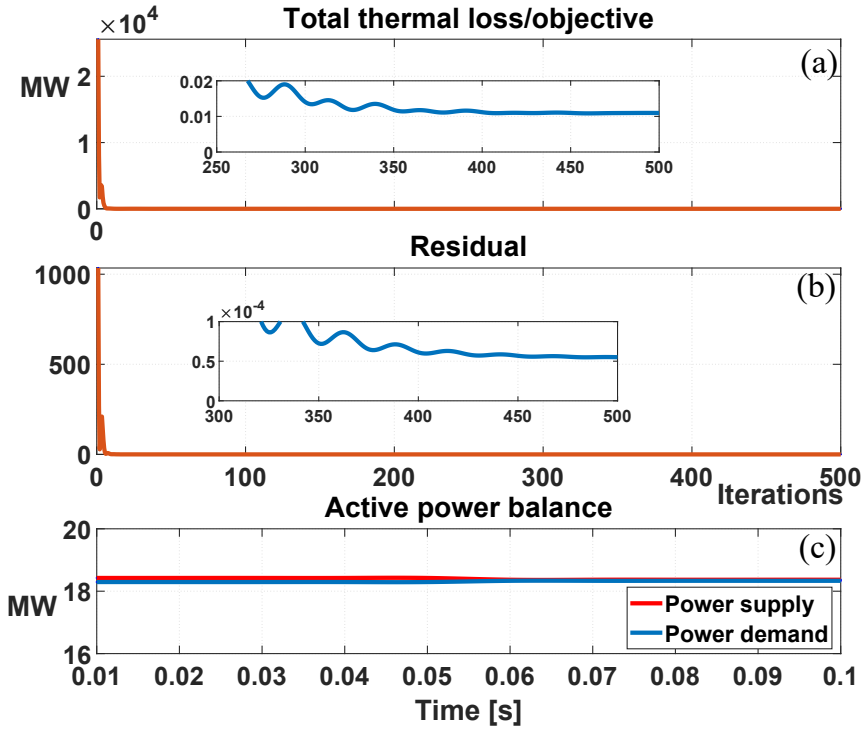

Figure 3.12: (a) Objective function value/losses (b) residual and (c) active power balance during sudden DER trip at bus 207

margins as validated in reference [30]. Hence, the computation of optimal DER set points is very fast for the Brazilian 136-bus network. Thus, the proposed control strategy caters for the highly variable power entities for the seamless and efficient operation of the DN.

3.6 Summary

This section proposes a novel method to solve the optimal control problem formulated for an active DN. Kron reduction is utilised to eliminate the passive components of the network, thus enhances the scalability of the algorithm to large scale (MW scale) electric distribution grids. The control problem is formulated an optimization problem in which the constraint capture the fast dynamics of sources and loads and impose bounds on the bus voltage magnitudes. A novel variable decomposition technique is introduced to tackle the tight spatial and temporal couplings in the dynamic constraints. Moreover exact convex relaxation techniques are applied to overcome the non-convex bus voltage lower bound constraint. The scalability, feasibility and superior convergence of the algorithm is demonstrated via simulation studies on practical DNs.

Chapter 4

Conclusions

The modern electric distribution grid is facing unprecedented changes in the source and load side. These two ends are now dictated by sophisticated power electronic based low inertia converters such as inverters (on the source side for Solar PV interconnection) and rectifiers (for EV battery charging). Moreover the DN is 'weak' (due to higher R/X ratio) and susceptible to higher voltage/frequency fluctuations during perturbations in sources and loads, violating the revised guidelines listed in IEEE 1547 standard. Unfortunately the existing structure of the DN is not expected to change at pace to mitigate these challenges. Moreover the existing state-of-the-art techniques (VVCs) such as shunt capacitive banks, transformer online tap changers etc are proven to be ineffective in tackling this issue and sometimes tend to degrade the quality of the voltage. Hence, we investigate into utilising the DER inverters to provide support in stabilising system voltage and during the events which can cause severe voltage fluctuations.

4.1 Contributions

In face of these challenges, the contributions of this thesis can be summarised as follows:

- Formulating the control problem for a DN as an LQR and proposing solution based on least squares. A decentralised communication architecture is proposed for the set point communication in the DN by leveraging on the sparsity of the gain matrix.
- A DP programming based solution is also proposed for the LQR formulated for the DN. superior set point tracking capability of the algorithm is proven by simulations and voltage

oscillations are damped by fine tuning the state penalties.

- The optimal control problem for the DN is formulated as a constrained optimisation problem which captures the fast dynamics of the system and includes bounds on voltage magnitudes. Kron reduction is applied to eliminate passive components of the electric network as control actuations are performed at the DER buses. This enhances the scalability of the algorithm to large scale (MWs) DNs.
- Spatial and temporal coupling between subsystems are decoupled by a strategic decomposition technique. This decoupling and the application of ADMM enable each subsystem agents to perform independent computations with minimal information exchange with other DER nodes.
- Non-convexities introduced due to the bus voltage lower bound magnitude constraint is tackled by proposing exact convex relaxations utilising S-procedure and Schur's compliment. This guarantees global convergence of the ADMM solver and feasibility of voltage bounds.
- Showcasing the effectiveness, scalability, feasibility and global convergence of the proposed algorithm by simulation studies on realistic 136-bus Brazilian distribution grid.

4.2 Future work

The proposed constrained optimisation based control algorithm is effective in tackling the voltage stability problem in the DN while preserving the power supply and demand balance. The possible extensions to this work are listed as follows:

- This presented algorithm is applicable only for 3-phase balanced DNs. As a future work, this can be extended to unbalanced 3-phase DNs as well. This can initiated by investigating on modifying the Kron reduction technique for unbalanced networks.
- A more generalised load model, such as constant impedance, current and power (ZIP) model can be included while mathematically modelling the DN.
- Extension of the algorithm to DC distribution networks.
- Extending the convex relaxation and decomposition techniques to include demand response and fault mitigation in the DN.

Bibliography

[1] F. Ahamed and P. Srikantha, "Optimal decentralized control of islanded microgrids via cyber interactions," in *2020 IEEE Power Energy Society Innovative Smart Grid Technologies Conference (ISGT)*, 2020, pp. 1–5.

[2] L. Luo and S. V. Dhople, "Spatiotemporal model reduction of inverter-based islanded microgrids," *IEEE Transactions on Energy Conversion*, vol. 29, no. 4, pp. 823–832, 2014.

[3] F. Ahamed and P. Srikantha, "Finite horizon optimal control with voltage regulation[submitted]," *IEEE Transactions on Smart Grid*, 2021.

[4] Z. K. Pecenak, J. Kleissl, and V. R. Disfani, "Smart inverter impacts on california distribution feeders with increasing pv penetration: A case study," in *2017 IEEE Power Energy Society General Meeting*, 2017, pp. 1–5.

[5] P. Kundur, "Power system stability," *Power system stability and control*, pp. 7–1, 2007.

[6] J. W. Simpson-Porco, F. Dörfler, and F. Bullo, "Voltage stabilization in microgrids via quadratic droop control," *IEEE Transactions on Automatic Control*, vol. 62, no. 3, pp. 1239–1253, 2017.

[7] Y. Khayat, M. Naderi, Q. Shafiee, Y. Batmani, M. Fathi, J. M. Guerrero, and H. Bevrani, "Decentralized optimal frequency control in autonomous microgrids," *IEEE Transactions on Power Systems*, vol. 34, no. 3, pp. 2345–2353, 2019.

[8] M. Ashabani, Y. A. . I. Mohamed, M. Mirsalim, and M. Aghashabani, "Multivariable droop control of synchronous current converters in weak grids/microgrids with decoupled dq-axes currents," *IEEE Transactions on Smart Grid*, vol. 6, no. 4, pp. 1610–1620, 2015.

[9] M. M. Bijaieh, W. W. Weaver, and R. D. Robinett, "Energy storage requirements for inverter-based microgrids under droop control in d-q coordinates," *IEEE Transactions on Energy Conversion*, vol. 35, no. 2, pp. 611–620, 2020.

[10] F. Chen, M. Chen, Q. Li, K. Meng, Y. Zheng, J. M. Guerrero, and D. Abbott, "Cost-based droop schemes for economic dispatch in islanded microgrids," *IEEE Transactions on Smart Grid*, vol. 8, no. 1, pp. 63–74, 2017.

[11] M. Sinha, F. Dörfler, B. B. Johnson, and S. V. Dhople, "Uncovering droop control laws embedded within the nonlinear dynamics of van der pol oscillators," *IEEE Transactions on Control of Network Systems*, vol. 4, no. 2, pp. 347–358, 2017.

[12] B. Pang and Z. P. Jiang, "Adaptive optimal control of linear periodic systems: An off-policy value iteration approach," *IEEE Transactions on Automatic Control*, vol. 66, no. 2, pp. 888–894, 2021.

[13] A. H. Etemadi, E. J. Davison, and R. Iravani, "A decentralized robust control strategy for multi-der microgrids—part i: Fundamental concepts," *IEEE Transactions on Power Delivery*, vol. 27, no. 4, pp. 1843–1853, 2012.

[14] M. Mallick and P. Srikantha, "Optimal decentralized microgrid coordination via the schur's complement and s-procedure," *IEEE Transactions on Smart Grid*, vol. 11, no. 1, pp. 379–390, 2020.

[15] B. Zhang, A. Y. S. Lam, A. D. Domínguez-García, and D. Tse, "An optimal and distributed method for voltage regulation in power distribution systems," *IEEE Transactions on Power Systems*, vol. 30, no. 4, pp. 1714–1726, 2015.

[16] Q. Peng and S. H. Low, "Distributed algorithm for optimal power flow on a radial network," in *53rd IEEE Conference on Decision and Control*, 2014, pp. 167–172.

[17] R. Hostettler, "Basics of sensor fusion," 2018.

[18] H. Farhangi, "The path of the smart grid," *IEEE Power and Energy Magazine*, vol. 8, no. 1, pp. 18–28, 2010.

[19] S. Boyd, S. P. Boyd, and L. Vandenberghe, *Convex optimization*. Cambridge university press, 2004.

[20] B. Abdolmaleki and Q. Shafiee, "Online kron reduction for economical frequency control of microgrids," *IEEE Transactions on Industrial Electronics*, vol. 67, no. 10, pp. 8461–8471, 2020.

[21] Y. Lin, B. Johnson, V. Gevorgian, V. Purba, and S. Dhople, "Stability assessment of a system comprising a single machine and inverter with scalable ratings," in *2017 North American Power Symposium (NAPS)*, 2017, pp. 1–6.

[22] F. Dorfler and F. Bullo, "Kron reduction of graphs with applications to electrical networks," *IEEE Transactions on Circuits and Systems I: Regular Papers*, vol. 60, no. 1, pp. 150–163, 2013.

[23] S. V. Dhople, B. B. Johnson, F. Dörfler, and A. O. Hamadeh, "Synchronization of nonlinear circuits in dynamic electrical networks with general topologies," *IEEE Transactions on Circuits and Systems I: Regular Papers*, vol. 61, no. 9, pp. 2677–2690, 2014.

[24] L. N. Ochoa and J. Quiros-Tortos, "Advanced modelling of smart distribution networks using opendss," 2015.

[25] M. Rasheduzzaman, J. A. Mueller, and J. W. Kimball, "An accurate small-signal model of inverter- dominated islanded microgrids using *dq* reference frame," *IEEE Journal of Emerging and Selected Topics in Power Electronics*, vol. 2, no. 4, pp. 1070–1080, 2014.

[26] *Micro-Phasor Measurement Unit*, Powerside, 2020.

[27] "IEEE standard for interconnection and interoperability of distributed energy resources with associated electric power systems interfaces," *IEEE Std 1547-2018 (Revision of IEEE Std 1547-2003)*, pp. 1–138, 2018.

[28] C. L. Masters, "Voltage rise: the big issue when connecting embedded generation to long 11 kv overhead lines," *Power Engineering Journal*, vol. 16, no. 1, pp. 5–12, 2002.

[29] J. R. Mantovani, F. Casari, and R. A. Romero, "Reconfiguração de sistemas de distribuição radiais utilizando o critério de queda de tensão," *Controle and Automacao*, pp. 150–159, 2000.

[30] J. P. Carvallo, P. H. Larsen, A. H. Sanstad, and C. A. Goldman, "Load forecasting in electric utility integrated resource planning," Berkeley CA, Tech. Rep., 2016.